Intra-interstadial environmental changes in Last Glacial loess revealed by molluscan assemblages from the Upper Palaeolithic site of Amiens-Renancourt 1 (Somme, France)

Olivier Moine, Pierre Antoine, Sylvie Coutard, Gilles Guérin, Christine Hatté, Clément Paris, Ségolène Saulnier-copard

Intra-interstadial environmental changes in Last Glacial loess revealed by molluscan assemblages from the Upper Palaeolithic site of Amiens-Renancourt 1 (Somme, France)

A molluscan record depicts intra-interstadial environmental phases

OLIVIER MOINE[1,*], PIERRE ANTOINE[1], SYLVIE COUTARD[3,1], GILLES GUÉRIN[2], CHRISTINE HATTÉ[2], CLÉMENT PARIS[3,4], SÉGOLÈNE SAULNIER-COPARD[1]

[1] UMR 8591 CNRS Université Paris 1 UPEC, Laboratoire de Géographie Physique: Environnements Quaternaires et Actuels, 1 place Aristide Briand, 92195 Meudon, FRANCE

[2] Laboratoire des Sciences du Climat et de l'Environnement, UMR 8212 CEA CNRS UVSQ, Université Paris-Saclay, 91191 Gif-sur-Yvette, FRANCE

[3] Institut National de Recherches Archéologiques Préventives, 80440 Glisy, FRANCE

[4] Archéologies et Sciences de l'Antiquité, UMR 7041 CNRS Université Paris 1 Université Paris Nanterre Ministère de la Culture, Université Paris 8 INRAP, 92023 Nanterre, FRANCE

* Corresponding author

ABSTRACT: The Amiens-Renancourt 1 site recently yielded one of the most important Upper Palaeolithic Human occupations of northern France by the number of flint artefacts and especially by the presence of Venus figurines. All the material comes from a single archaeological layer located in a tundra gley bracketed by loess units. A multi-proxy study combining a detailed stratigraphy, luminescence and radiocarbon datings and high-resolution (5 cm/sample) grain size and molluscan analyses was therefore carried out to reconstruct and date the associated environmental changes and to determine the exact context of the Human occupation. The chronological frame thus established supports the correlations of the archaeology-bearing tundra gley and of an underlying arctic brown soil with Greenland interstadials GI-4 and GI-3. Composition changes in the molluscan population enabled the identification of transitional and optimum phases and sub-phases within these two pedogenetic horizons. A conceptual correlation model linking molluscan phases with millennial-timescale variations of Greenland ice-core and Sieben Hengste speleothem climate records is proposed. The Human occupation appears contemporaneous to the end of the stadial-interstadial transition of GI-3. Synchronous in Amiens-Renancourt 1 and Nussloch, subsequent micro-gleys may also result from a regional/global forcing. Such a level of detail is unprecedented in a loess sequence.

KEYWORDS: Terrestrial molluscs, Loess, Upper Weichselian, Interstadial, Upper Palaeolithic

Introduction

In continental Europe, only a few (sub)continuous speleothems and sedimentological, pollen and diatom records from lacustrine and peat deposits document the environmental impact of the millennial-timescale milder oscillations, i.e. interstadials, of the last glacial period (Weichselian) north of the Mediterranean domain (Ampel et al., 2010; Luetscher et al., 2015; Fankheuser et al., 2016; Sirocko et al., 2016; Duprat-Oualid et al., 2017).

Conversely, loess deposits cover vast areas in European plains (Lehmkuhl et al., 2021) and offer numerous sequences showing alternations of loess units and pedogenetic horizons, i.e. tundra gleys or arctic/boreal brown soils (Antoine et al., 2001, 2013, 2014; Jary & Ciszek, 2013; Meszner et al., 2013; Haesaerts et al., 2016; Zens et al., 2018), which respectively deposited during stadials and formed during interstadials (Antoine et al., 2009). This scheme is particularly well-expressed between 35 and 20 ka owing to high sedimentation rates, i.e. about 1 m/ka, and supported by radiocarbon chronologies derived from classical (charcoal, bones, terrestrial mollusc shells) or new (earthworm calcite granules, *n*-alkanes) dating materials (Haesaerts, 2009; Moine et al., 2017; Újvári et al., 2017; Zech et al., 2017).

Contrary to pollen, terrestrial mollusc shells are present in most European loesses (Ložek, 1990). Their 5-40 % calcium carbonate ($CaCO_3$) content (Bosq et al., 2020) favoured both shell construction and preservation, but also the preservation of bone remains in Human occupation layers as well. As assemblages of these organisms are highly sensitive to their medium, they are well-suited to reconstruct millennial timescale palaeoenvironmental changes (e.g. Moine et al., 2008, 2011; Sümegi et al., 2019). They thus provide a useful complement to the chronostratigraphical frame for Middle and Upper Palaeolithic sites of northern France (Antoine et al., 2016).

Continuous molluscan records compiled for the 35-20 ka period revealed a similar environmental response to stadial-interstadial cycles across western Europe. Increases in both the total abundance of molluscs and the proportions of hygrophilous and palustral species respectively indicate warmer and more humid conditions during the formation and degradation of tundra gley horizons (Remy, 1969; Kerney, 1971; Schiermeyer, 2000; Moine et al., 2008, 2011). The disappearance of the most vegetation-requiring taxa systematically leads to a richness minimum at the top of tundra gleys interpreted as a harmful effect of ground ice on vegetation (Moine, 2014). In northern France, due to the poor mollusc diversity, this effect is less marked and a few species may even briefly appear at the basis of tundra gleys, indicating a short phase of vegetation improvement following harsh stadial conditions.

The Amiens-Renancourt 1 site offered us a new opportunity to document environmental changes associated with stadial-interstadial cycles with a time resolution rarely reached until now but which is necessary to characterise features specific to each cycle and event. This site also yielded the youngest Gravettian occupation of northern France preceding the abandonment of the region during the Last Glacial Maximum (LGM) (Antoine et al., 2016). Its study will thus also allow for the precise positioning of the archaeological layer in its climatic and environmental context.

This is thus a fundamental test to demonstrate that such an approach may improve correlations between archaeological layers and regional or global climate and environmental

records. Such correlations basically rely on the relative – by typology – or absolute – by radiocarbon or thermoluminescence – dating of the archaeological material, especially when the stratigraphy has been reworked, is unclear or complex and environmental proxies are absent or inconclusive. However, combining high resolution palaeoenvironmental information from bioindicators for open air sites located in clearly stratified loess sequences may allow much more precise correlations. Reaching the expected (multi-)centennial-timescale will definitely deepen the comprehension of the relationships between climate and human settlements in the European Plain during the last glacial period.

Site settings

The archaeological site of Amiens-Renancourt 1 is located in northern France (Fig. 1) at the edge of the western suburb of Amiens in the Renancourt district (49°54'5.21"N; 2°15'50.58"E). The excavation is located on the left-hand side of the Somme River valley, several meters above the level of its present alluvial plain, at the foot of the north exposed slope of a slight promontory separating the Grâce dry valley from the Selle River valley (Fig. 2).

The most complete loess succession is 6.75-m-thick and overlies a chalky flint gravel bed reached at a depth of 8.3 m using a manual auger (Fig. 3). No Quaternary sediments are found below this gravel bed. It overlies the bedrock constituted of Upper Cretaceous chalk outcropping westward at short distance and constituting the promontories that separate the different valleys (Kuntz & Dupuis, 1972).

The first archaeological discoveries in the surroundings date back to the beginning of the 20th century (Commont, 1913) owing to the numerous brickearth quarries in operation at that time. A concentration of Palaeolithic flint artefacts and large mammal bone remains was excavated on this occasion in the former Devalois quarry, but then lost. Fortunately, a new concentration, named Amiens-Renancourt 1, was discovered in 2011. Excavated every year since, the archaeological layer has already yielded many horse bone fragments, thousands of lithic remains attributed to the Recent-Final Gravettian technocomplex as well as ornamental items and several Venus figurines in chalk (Paris et al., 2017, 2019).

Based on these archaeological discoveries, Amiens-Renancourt 1 is thus one of the best preserved and most important Gravettian sites for northern France (Paris, 2020), and is even unique regarding the presence of Venus figurines. It is clearly positioned in the stratigraphy, almost undisturbed and with a very limited vertical dispersion. The high-resolution palaeoenvironmental study of this site, along with an adequate chronology, will thus contribute to documenting the impact of the millennial-timescale climate variability on continental loess environments and to exploring their relationship with this Human settlement.

Material and methods

Sampling strategies

The studied profile was positioned on a side of the excavated area so that it passes through the archaeological layer, which can be optimally associated with palaeoenvironmental proxies.

After a careful cleaning of the profile, a precise drawing of the sequence was made at the scale 1:20 annotated with pedostratigraphic features and the position of all the samples (Fig. 3). Following the continuous column sampling (CCS) established by Antoine et al. (2009), 48 samples were collected for grain size analyses by cutting successive 5-cm-thick and 200-g-large slices of sediment, as well as 44 5-cm-thick and 10-litre-large samples for molluscan analyses taken side by side in parallel (Fig. 3) for precise comparisons. Samples (H: -60/-65, H: -65/-70, H: -70/-75) located at the base of the upper profile close to and within the archaeological layer were taken afterwards during the excavation of the square crossed by the profile. As their volume was respectively 30, 20.25 and 16.80 litres of sediments, their molluscan abundances were normalised to 10 litres to be comparable with those of the other samples.

In addition, 6 samples were taken for optically stimulated luminescence (OSL) datings using copper cylinders (L = 14 cm, Ø = 3.5 cm) hammered horizontally into the sediment. After extraction they were sealed at both ends to prevent exposure to light. To measure dosimetric parameters, about 2 kg of the sediment were taken for each sample in a radius of 30 cm around each cylinder. Ten radiocarbon (hereafter ^{14}C) datings were also performed on samples of earthworm calcite granules (hereafter ECG) extracted from molluscan samples following the methodology of Moine et al. (2017) to complete the four obtained on bone, burnt bone and charcoal fragments from the archaeological layer (Paris et al., 2013, 2017). All dating samples were distributed throughout the record to constrain the age of the archaeological layer and of the main pedostratigraphic horizons of the studied part of the sequence.

Analytical protocols

Granulometry

Grain size analyses were performed on 2 to 5 g homogenised samples using a Beckman Coulter LS1330XR laser particle size analyser. The samples were first dispersed by sodium hexametaphosphate (5 ‰) during a period of one night in a rotating agitator, and then sieved at 160 µm to remove the coarse fraction including non-sedimentary Fe-Mn concretions, calcified roots and shell fragments that may bias the analysis. The coarse fraction was dried and weighed. For the decarbonated analyses, carbonates were removed using HCl (4 %) until the effervescence subsided. Then 1 to 2 ml of HCl (20 %) was added to check that the reaction was complete. The samples were rinsed by centrifugation before dispersion. Finer fractions were measured on the analyser at least three times to ensure good reproducibility. The limits of the grain size classes (clay: ≤ 6 µm; coarse silts: 20-61 µm; fine sands: 61-160 µm) were adjusted using the comparison between classical sieve-pipette and laser grain size analyses for a set of test samples from the loess sequence of Havrincourt about 60 km to the north-east (Antoine et al., 2014). The grain size index (hereafter GSI) defined as the ratio between coarse silts and fine silts plus clay (Rousseau *et al.*, 2002), which is sensitive to minor changes in the loess deposition dynamics, was calculated for the characterization of millennial-timescale climate changes, using class size limits defined for the laser particle size analyser (Antoine et al., 2009).

Luminescence dating

Luminescence analyses were performed on the fine (4-11 µm) quartz fraction. Preparation techniques followed usual procedures (Lang et al., 1996) and aliquots were prepared by settling of a 1 mg/ml suspension on 10 mm diameter stainless steel discs. The final quartz deposit was about 1 mg/cm^2. All luminescence measurements were performed using a Risø TL/OSL-DA-15 system equipped with blue (470 nm) light-emitting diodes and an IR (830 nm) laser diode (Bøtter-Jensen et al., 2002). The luminescence signals were detected through a 7.5 mm thick Hoya U-340 filter. Irradiations were performed with the ^{90}Sr/^{90}Y source of the TL-OSL reader (dose-rate on 01/01/2015 was 0.132 Gy/s).

The determination of equivalent doses was achieved using a single-aliquot regenerative-dose (SAR) procedure (Murray & Wintle, 2000). We used a measurement protocol identical to the SAR datings of quartz from Havrincourt loess (Guérin et al., 2017) as all samples have an OSL behaviour close to those of this site. Thus, the parameters of the SAR protocol were fixed individually for each sample so as to satisfy the preheat plateau test performed for preheat temperatures ranging from 180 to 320°C with 20°C steps. For all samples it was checked that the recycling ratio was unity within a few percent as well as the dose recovery test (Murray & Wintle, 2003). The alpha efficiency factor was set to 0.0420 ± 0.0020, the mean value measured on quartz from Havrincourt loess.

Annual dose rates were calculated using the data in table 1 and the last revised conversion factors (Guérin et al., 2011). The contribution of cosmic rays was calculated using the depth from the surface and a sediment density of 2 (Prescott & Hutton, 1994). U, Th and K concentrations were measured on the sediment samples taken around the OSL cylinders. Prior to gamma spectroscopy, the sediment was dried for 3 days at 105°C. Th and K activities were calculated using the specific activities of ^{234}Th, ^{228}Ra and ^{40}K, the latter only used for K. The water saturation content was measured for each sample and the incidence of moisture was calculated by assuming a mean water content of the sediment since its deposition between 60 and 100 % of the saturated value (Aitken, 1985).

Radiocarbon dating

For the archaeological layer, four samples (two bones, one burnt bone and one charcoal) were carefully selected for radiocarbon dating. Earthworm calcite granules were also selected following the protocol of Moine et al. (2017). For each molluscan sample, the 50 selected granules ($0.8 < Ø < 1$ mm) provided between 50 and 70 mg of $CaCO_3$. Radiocarbon measurements were performed in Poznan, Saclay and Lyon radiocarbon laboratories (Tab. 2). From the basal auger sediment sample, 3 granules were extracted for each of the three aliquots, providing between 1.1 and 1.51 mg of $CaCO_3$. Given the small volume of the sediment sample, the minimum size limit of selected granules was lowered to 0.5 mm. They were treated at LSCE, Gif-sur-Yvette (GifA/ECHo prefixes as chemistry ID and measurement ID respectively) according to the same chemical protocol. CO_2 evolved from carbonate acid attack was collected and flame-sealed in Pyrex tubes. Physical measurement was handled on the CO_2 gas itself (no graphitization step) by ECHoMICADAS (Synal et al. 2007; Tisnérat-Laborde et al., 2015) through the gas source (Ruff et al., 2007). This procedure makes it possible to measure samples as small as some dozens of micrograms of carbon.

Malacology

Sediment samples taken for the molluscan analysis were wet sieved on a 425 µm mesh and then dried. All useful shells and fragments were sorted, identified, counted and stored. The number of individuals per taxa was estimated according to Ložek (1964). Taxonomic attributions were based on Welter-Schultes (2012), the results of Nekola et al. (2015) for *Pupilla* species and the latest additions to the MolluscaBase (https://molluscabase.org/), and the ecological classification of taxa followed the groups established by Ložek (1964) and Puisségur (1976).

Results

Stratigraphy and sedimentology

According to the field description (Fig. 3), five sub-sequences can be distinguished:

- Sub-sequence I (unit 13 to 12) is made of loessic material partly reworked by hillwash processes and accumulated at the foot of the slope directly on the chalk bedrock, testifying to the occurrence of a major erosion event directly preceding the deposition of the first sandy loess of unit 13. The decreasing content in chalk granules and gelifracted flint fragments from the base to the top suggests that the contribution of the bedrock, eroded on the overlooking plateau, progressively decreased with the increasing loess cover deposition in the area. Unit 12 features are characteristic of a tundra gley horizon;

- Sub-sequence II (unit 11 to 6) is made of homogeneous loess units alternating with a weakly developed arctic brown soil (unit 10), a tundra gley (unit 8) and two micro-gleys. Its lower boundary is marked by the onset of both high GSI values and of an increasing trend in clay, suggesting an enhanced contribution of aeolian deposition processes (Fig. 4). In the absence of a synchronous GSI decrease, the decrease in fine sand percentage in the middle of unit 11 associated with the disappearance of sandy layers probably indicates the end of hillwash processes. A few meters away from the profile, unit 10 turns into a tundra gley horizon. Locally, its brownish facies may thus result from a better drainage favouring oxidation processes owing to a steeper slope. This recalls the BS5 units described at Ringen as an "intermediated tundra gley/boreal soil" (Zens et al., 2018). The archaeological layer is in the median part of the tundra gley (unit 8). Each of these two horizons is characterised by fine sand and GSI decreases with minima occurring 5-10 cm below the surface of unit 10 and 10-15 cm above that of unit 8. Slight decreases in the fine sand percentage are associated with the micro-gley located in the middle of unit 7 and in the thin upper tundra gley horizon (unit 6), whereas GSI values respectively show a plateau and an increase;

- Sub-sequence III (unit 5 and 4) is made of laminated sandy loess with cryo-desiccation micro-crack levels corresponding to small (Ø ~20-30 cm) polygons. Its sharp lower boundary and the associated GSI increase (Fig. 4) highlight a rapid change toward a stronger loess deposition dynamics;

- Sub-sequence IV (unit 3 and 2) is made of homogenous loess. It began with an erosive humid and cold event marked by a humic tundra gley in which one ice-wedge cast was

observed. The loess deposition dynamics reverts to similar conditions to those prevailing during sequence II, albeit much more stable;

- Sub-sequence V (unit 1 and 0) is made of two horizons belonging to the Lateglacial/Holocene soil complex strongly eroded by anthropogenic processes (agriculture).

Chronology

Distributed from the top of unit 12 to the top of unit 7, ECG ^{14}C ages range from 40926-45484 to 26036-26929 cal BP without inversions (Tab. 2; Fig. 4). Scattered between 40926-45484 and 30667-31646 cal BP, the three ages provided by the three small aliquots of the lowermost sample indicate that ECG of different ages were gathered along the slope by reworking processes. The younger one provides a minimum age estimate of the reworking phase. Such a mix explains the gap of about 6 ka that separates both ages from unit 11. The two lowermost ages of column B and the two oldest ones of the auger sample were therefore rejected. The ^{14}C age obtained on earthworm calcite granules in the archaeological layer is in very good agreement with those obtained on burnt bone and charcoal. This demonstrates the reliability of this material for ^{14}C datings in loess contexts from north-western Europe. The other two ages obtained on bone appear significantly younger (no recovery between their 2σ age ranges and that of the ECG ^{14}C of the archaeological layer). Such shifts between ages obtained from different materials of a unique layer often occur in archaeological contexts. They may result from the quality of the samples or from the dated carbon fraction, which depends on the nature or the preservation state of the samples. The two ^{14}C ages (Lyon-632 and Lyon-633) obtained on an isolated bone found in a test pit in 1997 about 100 m SE of the excavation site (Fagnart et al., 2013) demonstrate the occurrence of erosional events and hillwash processes during the deposition of the thick laminated loess of sequence III. The topographically higher position of this bone also suggests an occupation of the area by prehistoric humans that largely exceeded the limits of the excavation. According to the uppermost ^{14}C, i.e. 26036-26929 cal BP, sequence II should end around 26.5-26 ka. Statistically different, the ^{14}C ages obtained in unit 10 and 8 confirm the occurrence of two independent pedogenic phases.

Distributed between units 13 and 7, OSL ages range from 31.0 ± 1.6 to 27.2 ± 1.5 ka (Tab. 1). Both ^{14}C and OSL age ranges are thus in good agreement. The uppermost one, i.e. REN1 14-03 (27.6 ± 1.4 ka), is slightly younger than the closest ^{14}C age of sample H: -15:-10 (26036-26929 cal BP), though this difference is not statistically significant. Nor is the apparent shift of the youngest OSL age of the archaeological layer, i.e. REN1 14-04 (27.2 ± 1.5 ka), which takes the error bars into account. The discrepancy is greater for the OSL age located in unit 13. Sample REN1 15-01 appears significantly younger than sample REN1 14-02 located above (Tab. 1). However, its water content (23.3 ± 2.3 %), which is significantly lower than that of all the other samples, is certainly incorrect and was therefore assumed to result from the destructuring of the sample between the field and the laboratory, leading to a decreased capacity to absorb water. Recalculated with the water content value of a physically close sample taken on another profile of the site (Fig. 3, Tab. 1), REN1 15-01* yields an age of 30.5 ± 2.0 ka, close to that of sample REN1 14-02 and to the ^{14}C of sample A: 0-20 (30667-31646 cal BP). It is assumed here that the strong reworking undergone by unit 13 may have reduced its porosity and water absorption capacity, leading to younger ages. Furthermore, the

lower positions of samples REN1 15-01* and A: 0-20 suggest a rapid deposition of reworked units 13 and 12, possibly during Greenland interstadial (GI) 5.1.

Consequently, the Amiens-Renancourt 1 loess sequence covers the period between about 31 and 22 ka. Its four main pedogenic horizons are synchronous with GI-5.1, GI-4, GI-3 and GI-2, the third one including a unique archaeological layer solidly dated around 27.5-28 ka (Fig. 4).

Malacology

The number of individuals per assemblage (hereafter abundance) varies between 8 and 3855, and the number of taxa (hereafter richness) between 3 and 6 (Tab. 3; Fig. 5). Extreme values of both parameters are similar to those from other northern France molluscan records (Moine, 2008; Moine et al., 2011). Moreover, owing to the occurrences of *Arianta arbustorum*, *Vallonia costata*, *Punctum pygmaeum* and *Clausilia rugosa parvula*, the composition of the molluscan fauna is in agreement with the position of the site at the boundary between the western and central malacological domains (Moine, 2014). The poor diversity and the ecological preferences of the few molluscan taxa (Tab. 4) almost always reflect a micro-environmental mosaic dominated by damp areas in which palustral and dry loci of variable extension occur. Moreover, the limited changes in the composition of the molluscan fauna and in taxa relative abundances (Fig. 5) indicate that the vegetation cover was most of the time discontinuous and poorly diversified, with only short phases of densification possibly accompanied by isolated patches of shrubs. However, despite the relative stability of the composition of the molluscan fauna, the thorough observation of variations in absolute and relative taxa abundances revealed the existence of four types of phases (Tab. 5) succeeding in a pattern of seven cycles (C1-7) (Fig. 5).

Phase I

All the samples attributed to this type of phase are located in homogeneous (units 11, 9 and 7) or laminated (unit 5) loess units. Their very low abundance rarely exceeds 100 individuals (Tab. 5, Fig. 5). As most taxa of the site are able to survive freezing temperatures down to -12 to -15°C (Ansart et al., 2014), cold temperatures during the activity period most probably limited the development of the molluscan population during these phases. Indeed, rearing experiments at less than 15°C attempted during the cited study proved to be ineffective.

The relative abundances of dominant taxa indicate that the environmental conditions attributed to phase I differ slightly from one cycle to another. They can be rather dry (cycles C2 and C7), damp (cycles C3, C5 and C6), or well-balanced between the different components (dry, damp, palustral) of the micro-environmental mosaic (cycle C4). Although phase I molluscan faunas almost always reflect a discontinuous and poorly diversified vegetation cover, occasional occurrences of *Vallonia costata* indicate short phases of densification as during C2, C4 and C5.

Phase II

This type of phase is characterised by a simultaneous increase in all common taxa of the site, with a first weak ("start") sub-phase up to a few hundred individuals then a stronger ("acceleration") sub-phase up to several thousands. Moreover, as the hygrophilous species *Succinella oblonga* reacts more promptly and slightly more intensively than the others, it always predominates in phase II. The "start" sub-phase is common to all cycles from C2 to C6. It occurs at the top of loess units underlying the main pedogenic horizons in the full cycles C3 and C4, and in the micro-gleys and thin tundra gley of the incomplete cycles C2, C5 and C6. Although dominated by the palustral species *P. alpicola*, the sample of the uppermost micro-gley was included in phase II of cycle C6 given its 40 % of *S. oblonga* and low abundance. The "acceleration" sub-phase occurs only in the full cycles C3 and C4 and is located at the basis of the main pedogenic horizons (units 10 and 8).

In the full cycle C3, the "acceleration" sub-phase is also characterised by the appearance of the mesophilous species *Trochulus hispidus* and the presence of *Clausilia rugosa parvula* and *Punctum pygmaeum*, two vegetation-demanding species, which all benefit from the moderate moisture increase. In cycle C4, only *Trochulus hispidus* is present. During the "start" sub-phase of cycle C5 *Clausilia rugosa parvula* briefly occurs with half-forested species *Arianta arbustorum*. The richness thus increases from phase I to phase II. Consequently, both the increases in abundance and the progressive predominance of *S. oblonga* indicate a two-step increase in both temperature and moisture throughout phase II. A damp micro-environmental mosaic develops in which wet loci extend and the vegetation cover densifies including a few shrub patches during the "acceleration" sub-phase or from the "start" sub-phase.

In the uppermost sample of phase II in cycle C4, the taxa relative abundance remains the same as in the underlying one also included in the "acceleration" sub-phase, despite a sudden drop in species abundances. Contemporaneous to the dense archaeological layer, this abundance drop rather results from anthropic effects (trampling, etc.) than from a marked temperature decrease in such an improved climatic context.

Phase III

This phase occurs in the full cycles C3 and C4, and also possibly in cycle C1. In cycle C3, a "humid" sub-phase precedes a "dry" one. In the "humid" sub-phase, the total abundance is maximum and richness decreases mostly due to the disappearance of the vegetation-demanding taxa that appeared in phase II. *P. alpicola* prevails as it increases slightly more than slugs and *P. muscorum*. *S. oblonga* begins to decrease, slightly in C3 but much more in C4, i.e. in the sample overlying the archaeological layer. However, it remains unclear here whether this strong decrease results from environmental conditions or from the incapacity of *S. oblonga* to recolonize this anthropized area as all other dominant taxa return to almost the same level of abundance as before the Human occupation. During the "dry" sub-phase, the total abundance remains maximum, as *P. muscorum*, which predominates, and slug increases compensate the decreases in *S. oblonga* and *P. alpicola*. *T. hispidus* increases significantly but none of the vegetation-demanding taxa reappear.

Phase III occurs only in the arctic brown soil (unit 10) and in the tundra gley (unit 8). It is characterised by milder temperatures in C3 than in C4 and by a damp micro-environmental mosaic. During the "humid" phase, the extension of wet loci was maximum and more

prominent in C4 than in C3. This is coherent with the typical reduced facies of the tundra gley (unit 8) inherited from the waterlogging of the active layer which was less well drained than during the formation of the arctic brown soil (unit 10). During the "dry" sub-phase, most of the damp areas turn to dry ones, which become prominent, whereas wet loci only slightly regress. In the absence of aquatic taxa and of a marked micro-topography, the succession of a seasonal thaw followed by a drier phase during the activity period appears more probable than the persistence of localized water ponds or releases in a drier landscape to explain the persistence of wet loci. During both sub-phases, the vegetation remains discontinuous and poorly diversified, owing to the harmful effects of waterlogging and ice lenses on plant roots, as in other tundra gley horizons (Moine, 2014).

Phase IV

This phase only follows phase III in the full cycles C1, C3 and C4. As all taxa decrease, the total abundance drops strongly but remains above 500 individuals in most of the samples. As slugs decrease less sharply, their proportions peak and the taxon sometimes prevails as in cycle C3. Phase IV of cycles C1 and C3 takes place in the upper part of geliflucted tundra gley (unit 12) and arctic brown soil (unit 10). In cycle C1, the micro-environmental mosaic resembles that of phase III in cycle C3 despite lower temperatures. The co-dominance of *P. alpicola* and *P. muscorum* indicate the development of a micro-environmental mosaic with both wet and dry areas. The low proportion of the hygrophilous species *S. oblonga* suggests that water is restrained in delimited loci or in time, e.g. during the seasonal thaw, which fits with the geliflucted facies of unit 12. Though scarce, the occurrence of *Pisidium* sp. suggests at least temporary local ponds. As for the brief occurrence of *V. costata*, it indicates an increase in the herbaceous component of the vegetation cover in dry areas. In cycle C3, the micro-environmental mosaic appears well-balanced between dry, damp and wet areas. However, the vegetation remains sparse despite a moderately moist and stable soil resulting from a higher clay content which favoured the development of slugs.

Phase IV of cycle C4 takes place at the base of the homogeneous loess (unit 7) directly overlying the tundra gley (unit 8). The molluscan fauna reflects a cooling context and a damp micro-environmental mosaic in which wet loci tend to disappear. Only a slight increase in the herbaceous component is indicated by a brief occurrence of *V. costata* in the basal sample. This environmental trend is contrary to that observed in phase II. The presence of *Pisidium* sp. suggests the persistence of temporary ponds in the surroundings. Despite relatively high temperatures, the moderate moisture increase, the absence of water-driven sedimentological features and the resumption of loess deposition underline the limited seasonal water release but its possibly longer persistence during the activity period of the previous phase III.

Discussion

Stadial-interstadial cycles

The 5-cm sampling resolution of the Amiens-Renancourt 1 molluscan record provides a new opportunity to confirm the conceptual model linking palaeoenvironmental changes associated with loess-tundra gley alternations with Weichselian Upper Pleniglacial stadial-interstadial

cycles (Antoine et al., 2009) based on the combination of high resolution stratigraphy, grain size (Antoine et al., 2001; Rousseau et al., 2002) and molluscan (Moine et al., 2008) analyses at Nussloch (Rhine Valley, Germany). The correlation of large abundance increases, which occur in tundra gley horizons and imply milder temperatures, with interstadial phases (Moine et al., 2008) was recently confirmed by radiocarbon datings (Moine et al., 2017). Conversely, all low abundance samples from loess units were linked with stadial phases.

Furthermore, by combining the intra-interstadial environmental succession reconstructed from the molluscan record and its chronological frame, a correlation is proposed between molluscan phases and major variations of several high-resolution global and regional climate records. NorthGRIP (NGRIP) $\delta^{18}O$ and calcium ion concentrations ($[Ca^{2+}]$), hereafter dust concentration, in ice core records mostly reflect local temperature and atmospheric dust loading respectively (Rasmussen et al., 2004), whereas the Sieben Hengste (7H) speleothem $\delta^{18}O$ record reflects the balance between moisture reaching the site directly from the North Atlantic and by crossing the Alps from the south (Luetscher et al., 2015). Indeed, at the depth of the site (215 m below the ground surface), the temperature was assumed to be constant and $\delta^{18}O$ variations to result from precipitation isotope values, i.e. provenance. Luetscher et al. (2015) also pointed out that since the North Atlantic is the main moisture source in the northern Alps, the total moisture amount increases with its proportions.

Phase I

According to the cold temperatures implied by its low molluscan abundances, phase I is linked with stadials (Fig. 7). The molluscan assemblages of Amiens-Renancourt 1 reflect poor and discontinuous steppe/tundra vegetation. This is in agreement with the rare pollen data in loess sequences. North-eastward, Weichselian Upper Pleniglacial pollen samples from Kesselt (eastern Belgium) indicate a grass-dominated steppe (Bastin, 1969). Southward, Weichselian Middle Pleniglacial pollen samples, from Villiers-Adam (northern France), Upper Pleniglacial being sterile, also indicate a grass dominated vegetation with rare woody taxa resembling modern Nordic tundra (Limondin-Lozouet & Gauthier, 2003). At Amiens-Renancourt 1, owing to the low local richness, no cyclical variations of molluscan richness occur during stadials as in Nussloch, except brief occurrences of *V. costata* in phases I of C4 and C5 (Fig. 6). The ecological preferences of additional taxa present in Nussloch reflect a much more diversified vegetation with the presence of shrubs. The Bergsee Lake (Black Forest, Germany) pollen record shows a "steppe dominated landscape with some elements of boreal forest" during stadials, and GS-3 and GS-5.1 are distinguished by their maximum of xerophytic steppe element, i.e. *Artemisia* (Duprat-Oualid et al., 2017). Interestingly, the driest phases I at Amiens-Renancourt 1, i.e. in C2 and C7, are respectively correlated with these two stadials contemporaneous to HE 3 and 2 respectively, whereas at Nussloch molluscan richness maxima suggest a densification of the vegetation cover and increases in shrubs.

Phase II

Phase II, and especially its two sub-phases (start and acceleration), had not yet been precisely depicted. At Curgies (northern France), "MZ2" located at the basis of a tundra gley presents the characteristics of phase II, including a short occurrence of a vegetation-requiring species

typical of cold and wet mountain environments, i.e. *Columella columella* (see Moine et al., 2011). At Nussloch, only a "MP-3" phase with higher frequencies in hygrophilous *Succinella oblonga* was recognized (Fig. 6) and occurred within all tundra gley horizons and micro-gleys. Increases in the proportions of *S. oblonga* also preceded the high abundance "MP-0" phases at the basis of both G3 and G4 tundra gleys. It must be kept in mind here that hydromorphic processes leading to gley formation are linked to the functioning of a permafrost active layer and develop mainly downward in previously deposited sediments (Antoine et al., 2009). This can explain the apparent discrepancy between the two phases II taking place at the base of tundra gleys at Nussloch and in underlying loess at Amiens-Renancourt 1. Hence, as the large molluscan abundance increase occurs only during the "acceleration" sub-phase, "start" sub-phases are correlated with small excursions of 7H $\delta^{18}O$ towards less depleted values contemporaneous to limited NGRIP dust concentration decreases that precede GI-4 and GI-3 but also occur within GS-3 based on ^{14}C dating. As for "acceleration" sub-phases, they are linked with a subsequent increased shift in both 7H $\delta^{18}O$ and NGRIP dust concentration preceding GI-4 and GI-3. Active layer annual freeze-thaw cycles probably began during the "acceleration" sub-phase given its high abundances and trend toward palustral conditions. The 7H $\delta^{18}O$ record also indicates a larger and earlier moisture increase before GI-4 than before GI-3. In the absence of local effects, this may explain the greater thickness of both the arctic brown soil (unit 10) at Amiens-Renancourt 1 and G3 tundra gley at Nussloch compared to the above (unit 8) and G4 tundra gleys respectively (Fig. 6). At Amiens-Renancourt 1, the untypical arctic brown soil (unit 10) also implies reduced waterlogging periods and soil moisture content, and thus a limited harmful impact of diurnal freeze-thaw cycles on plant roots (Walker & Walker, 1991).

In addition, the richer molluscan fauna occurring in GI-4 phase II in both sites also suggest a greater lengthening of the growing season allowing for a more complex seasonal succession of vegetation resulting in an apparently more diversified micro-environmental mosaic. The occurrences of *Clausilia rugosa parvula* and *Punctum pygmaeum* in phase II of cycle C3 and C5 (only *C. r. parvula* for the latter) are also remarkable as original in northern France and as no other elements suggest their possible allochthonous or reworked origin in this sequence. Contrary to *Arianta arbustorum* and *Vallonia costata*, which are present eastward and southward in loess from the Paris Basin, *C. r. parvula* and *P. pygmaeum* are only known in the Rhine Valley during the Weichselian Upper Pleniglacial (Moine, 2014). Their discovery raises the question of whether they persist in cryptic refuge areas in the region or come from abroad and by which means of transport. Surprisingly, *P. pygmaeum* also occurs at Nussloch (Rhine Valley, Germany) only at the top of the loess underlying G3 tundra gley during the studied time interval. Otherwise, such scarce occurrences indicate cryptic populations that may have been missed elsewhere in the sequence whereas these rarer taxa were still living in the surroundings. The lack of precise knowledge on Last Glacial loess molluscan fauna still prevents any conclusion as to whether occurrences of *C. r. parvula* and *P. pygmaeum* at Amiens-Renancourt 1 result from brief passive colonization phases from the Rhine Valley by an efficient means of transport, or from active expansion phases from local cryptic refuges. Whatever the case, the development of shrub patches at Amiens-Renancourt 1 may have benefited from its position sheltered from (north-)western winds by the higher Ferme de Grâce plateau on the opposite slope of the Grâce valley (Fig. 2).

Phase III

In all Weichselian Upper Pleniglacial loess sequences where they have been detected, large abundances characteristic of phase III (e.g. "MP-0" phases at Nussloch) only occur in thick cryoturbated tundra gley horizons or arctic brown soils (Remy, 1969; Schiermeyer, 2000; Moine et al., 2008, 2011), and never in thin micro-gleys (Fig. 6). In most cases associated with maximum proportions in hygrophilous and/or palustral taxa, they formed during the functioning of the active layer, which requires milder temperatures (Moine et al., 2008; Antoine et al., 2009). This thus supports the correlation of the different phases III with interstadial phases marked by maximum $\delta^{18}O$ values and minimum dust concentration in NGRIP records (Fig. 7). Accompanying changes in the structure of the *Pupilla* populations support a lengthening of the activity period of snails over the year implying milder temperatures in spring, and to a lesser extent in autumn, rather than in summer (Moine et al., 2008, Moine, 2014). This is in agreement with palaeoenvironmental reconstructions from Les Echets (central-eastern France) diatom assemblages (Ampel et al., 2010) and modelling results from Flückiger et al. (2008). As already underlined above, interstadial environmental conditions did not favour the diversification of the vegetation, but at least benefited the development of *Betula* populations as recorded in the Bergsee Lake (Duprat-Oualid et al., 2017) but also in a tundra gley from the loess sequence of Kesselt (Bastin, 1969), most of the other tree taxa being allochthonous, e.g. *Pinus* (Duprat-Oualid et al., 2017).

Interestingly, the 7H $\delta^{18}O$ signal shifts back to its stadial level in the middle of GI-4 and GI-3. Slight decreases in NGRIP $\delta^{18}O$ values occur synchronously. The shift back to stadial values follows immediately in GI-3 but occurs after a period of stability in GI-4. Both interstadials have thus their own course and different palaeoenvironmental responses. During GI-4, the decrease in North Atlantic moisture supply whereas temperatures are still high probably explains the occurrence of an additional dry sub-phase after the humid one within phase III in the arctic brown soil (unit 10). During this dry sub-phase, the dust concentration in the NGRIP ice core remains low, which fits with minimum grain size values in Amiens-Renancourt 1. Owing to the strong cryoturbation of the top of thick tundra gley horizons that generally leads to their mix with the basis of the overlying loess unit (Fig. 6), this environmental phase has to our knowledge never been described up to now.

Finally, the correlation of phase III of cycle C1 must be considered with caution owing to the strongly cryoturbated facies of the sediment of the lowest tundra horizon (unit 12). A possible reworking of older material cannot be excluded though the composition changes in the molluscan fauna at the basis of the record appear realistic and the shells are well-preserved despite being sensitive to transport owing to their thinness.

Phase IV

As for phase III, pending phase IV is only linked with thick tundra gleys. Its large molluscan abundance decrease to minimum values reflects a strong temperature shift towards stadial levels, which obviously leads to correlating it to interstadial-stadial conditions characterised by a large decrease in the NGRIP $\delta^{18}O$ record. During phase IV of cycle C3, the molluscan abundance decrease is significantly sharper than during phase IV of cycle C4, which fits the quicker $\delta^{18}O$ decrease in GI-4 than in GI-3. Regarding the aeolian dynamics, the loess GSI, as

well as the fine sand percentage (Fig. 4), at the top of the arctic brown soil (unit 10) increases in parallel to the dust concentration at the top of GI-4 (Fig. 7).

Conversely, the link is not that clear in phase IV of cycle C4 which shows an almost flat loess GSI signal, and only a slight increase in the fine sand percentage, at the top of the upper tundra gley (unit 8), whereas the dust concentration increases at the same pace at the end of GI-3 as at the end of GI-4 (Fig. 7). Other striking features are the relatively high molluscan abundance, intermediate between interstadial and stadial values, and the high proportions in hygrophilous taxa throughout this phase IV, suggesting the persistence of a moisture supply, whereas 7H $\delta^{18}O$ values are the same for both phases IV. Up to now, these discrepancies remain unexplained, but interestingly the same evolution characterises this transition at the top of the upper tundra gley horizon at Amiens-Renancourt 1 and at the top of G4 tundra gley at Nussloch (Fig. 6), suggesting in both sites a similar forcing that affected neither NGRIP nor 7H records.

Early LGM interstadial-like oscillations

Owing to the reliable and precise radiocarbon chronology, more tenuous stratigraphical horizons than loess units and arctic brown soil/tundra gleys can be correlated between Amiens-Renancourt 1 and Nussloch sequences. Indeed, careful field observations revealed the presence at Amiens-Renancourt 1 of micro-gleys (Fig. 3, unit 6 and thin diffuse horizons with oxidation stains within units 7 and 11) presenting the same features as those already described in several profiles from Nussloch, i.e. P3 (Fig. 4). There, they are characterised by GSI minima (Antoine et al., 2009) and both increases in the percentage of hygrophilous taxa and decreases in molluscan richness (Moine et al., 2008). At Amiens-Renancourt 1, this concerns molluscan cycles C5 and C6 (Fig. 5). They are marked by a slowdown in the increasing trends of both GSI and the fine sand fraction (Fig. 4), increases in the percentage of hygrophilous and to a lesser extent of palustral taxa, a decrease in molluscan richness, slight and only in C5 as it is already minimum at the top of unit 7, and slight abundance increases (Fig. 5). These features are similar to those characterising the "start" sub-phase of stadial-interstadial transitions at the beginning of full cycles associated to the arctic brown (unit 10) soil and the tundra gley (unit 8). Further east, the loess section of Krems-Wachtberg (Austria) also exhibits supernumerary micro-gleys characterised by slight decreases in GSI and middle plus coarse sand values and similar, though weaker, trends in colorimetric parameters to those of tundra gleys (Sprafke et al., 2020). According to the correlations established with Greenland climate records, the micro-gleys IV-b and IV-d of profile KW-A 2015 could be contemporaneous of unit 6 and the diffuse horizon with oxidation stains of unit 7 at Amiens-Renancourt 1. In between at Remagen (Germany), recent high-resolution total organic carbon (TOC) measurements were performed along several cores drilled in a plateau loess sequence (Fischer et al., 2020). Along the thickest of these cores (REM 3), TOC increases of 0.1 to 0.3 % characterised pedogenetic horizons. Based on correlations with the RP1 profile located on the edge of the plateau and dated by radiocarbon and optically stimulated luminescence, excursions 10 and 9 associated with tundra gleys could be correlated with interstadials GI 4 and GI 3 respectively. Three weaker (0.4-0.5 %) TOC excursions (8, 7 and 6) were measured between GI 3 and the Eltville tephra dated around 24.3-24.4 ka (Zens et al., 2017). Though only excursion 6 appears associated with a tundra gley, all constitute potential equivalents for

Amiens-Renancourt and Nussloch micro-gleys, but require, as do the Krems-Wachtberg ones, direct radiocarbon dating to ensure precise correlations.

The comparison between the Nussloch GSI record and a few different ice, oceanic and continental proxy records of the Northern Hemisphere has highlighted the resemblance of their signals and suggests the occurrence of millennial-timescale variations between 28 and 20 ka. Their absence from the NGRIP $\delta^{18}O$ record, though present in the dust record, indicates that climatic cycles of minor amplitude and/or limited to the mid-latitudes occurred during the first half of the Last Glacial Maximum (Moine et al., 2017). However, both proxy sensitivity and chronological model precision still hamper their discrimination. Presently, although these tenuous changes in the composition of the molluscan fauna may be considered as a response to local changes, their resemblance and contemporaneity in both sites located about 500 km apart, as well as the similar trends of associated loess grain size variations with NGRIP dust concentration ones (Fig. 7), rather support that they result from global mid-latitude interstadial-like climate oscillations during the early Last Glacial Maximum.

Age and context of the Human occupation

Gravettian open-air sites are rare in northern France (Paris, 2020), and some of them found in loess sequences have been discovered in brownish loam units at the base of the Weichselian Upper Pleniglacial sequence, e.g. at Havrincourt (Antoine et al., 2014). However, despite the high resolution (5-cm-thick samples) of the molluscan records, the low sedimentation rate of these horizons prevents the precise reconstruction of associated palaeoenvironmental changes. Amiens-Renancourt 1 is thus the first site for which we have both a precise stratigraphical location and a favourable context for the preservation of carbonated proxies. The ^{14}C ages obtained on various materials (charcoals, burnt bones, bones, earthworm calcite granules) support the correlation of the Amiens-Renancourt 1 archaeological layer with the GI-3 interstadial (Rasmussen et al., 2014). Furthermore, after a precise description of the palaeoenvironmental evolution of the site, the relative position of the Human occupation within the succession of molluscan phases at the end of the "acceleration" sub-phase of phase II supports its occurrence at the end of the stadial-interstadial transition, during an optimum of vegetation diversification favoured by mild temperatures and moist conditions.

Conclusion

Our study is the first attempt to combine a high-resolution (5 cm) molluscan study with earthworm calcite granule radiocarbon dating throughout a calcareous loess sequence encompassing two Dansgaard-Oeschger (D-O) cycles and one important Palaeolithic occupation layer. It strengthens and refines the scheme of (multi-)centennial environmental phases succeeding during both interstadials and stadials established in northern France and Nussloch (Rhine Valley, Germany), and especially the role of milder and more humid conditions that progressively set in from the end of stadials to interstadial optimums. It allows for the characterization of the environmental context of a unique archaeological layer and its exact positioning at the end of the stadial-interstadial transition of a D-O cycle, and the highlighting of interstadial-like environmental changes during the Last Glacial Maximum.

In the future, such high-resolution studies of open-air sites will thus be crucial, not only to better constrain the millennial-timescale environmental dynamics, but also to specify the Human settlement dynamics in the cyclically changing environmental and climatic context of the end of the Last Glacial in the north-western side of the European periglacial domain.

Indeed, compared to studies carried out in caves, such a combination of palaeoenvironmental proxies and dating methods with high-resolution stratigraphy results in a better constrained chronology. Consequently, this type of high-resolution approach needs to be systematically applied in archaeological open-air sites presenting suitable characteristics such as a clear stratigraphical succession, no or minor reworking processes, a sufficient sedimentation rate, carbonated sediments, and an appropriate palaeontological content, as at Amiens-Renancourt 1.

Owing to the diversity of facies included in the Gravettian lithic techno-complex, the precise and respective chronological positioning of a maximum of well documented and typical archaeological layers from open-air sites in loess sequences appears as the best way to reconstruct the succession of Gravettian lithic trends that spread across the European Great Plain during the ten millennia preceding the Last Glacial Maximum.

Acknowledgements and funding. We thank both the Poznan Radiocarbon Laboratory and the LMC14 laboratory that undertook ^{14}C dating. Radiocarbon dating was supported by a CNRS project "Projets Exploratoires Premier Soutien" program and by CNRS ARTEMIS calls for ^{14}C dating. The first author would like to thank Léa Roth for her help in sorting the mollusc shells. The authors also thank Barna Páll-Gergely and an anonymous reviewer for their helpful comments that greatly improved the initial version of the manuscript.

Data statement

The data that support the findings of this study are available from the corresponding author upon reasonable request.

References

Aitken MJ. 1985. *Thermoluminescence Dating*. Academic Press: London.

Ampel L, Bigler C, Wohlfarth B, *et al*. 2010. Modest summer temperature variability during DO cycles in western Europe. *Quaternary Science Reviews* **29**: 1322–1327.

Ansart A, Guiller A, Moine O, *et al*. 2014. Is cold hardiness size-constrained? A comparative approach in land snails. *Evolutionary Ecology* **28**: 471-493.

Antoine P, Coutard S, Guérin G, *et al*. 2016. Upper Pleistocene loess-palaeosol records from Northern France in the European context: Environmental background and dating of the Middle Palaeolithic. *Quaternary International* **411**: 4–24.

Antoine P, Goval E, Jamet G, *et al*. 2014. Les séquences loessiques pléistocène supérieur d'Havrincourt (Pas-de-Calais, France) : stratigraphie, paléoenvironnements, géochronologie et occupations paléolithiques. *Quaternaire* **25**: 321–368.

Antoine P, Rousseau DD, Degeai JP, *et al*. 2013. High-resolution record of the environmental response to climatic variations during the Last Interglacial–Glacial cycle in Central Europe: the loess-palaeosol sequence of Dolní Věstonice (Czech Republic). *Quaternary Science Reviews* **67**: 17–38.

Antoine P, Rousseau D-D, Moine O, *et al*. 2009. Rapid and cyclic aeolian deposition during the Last Glacial in European loess: a high-resolution record from Nussloch, Germany. *Quaternary Science Reviews* **28**: 2955–2973.

Antoine P, Rousseau DD, Zöller L, *et al*. 2001. High-resolution record of the last Interglacial-glacial cycle in the Nussloch loess-palaeosol sequences, Upper Rhine Area, Germany. *Quaternary International* **76-77**: 211–229.

Bastin B. 1969. Premiers résultats de l'analyse pollinique des lœss en Belgique. *Bulletin de l'Association Française pour l'Etude du Quaternaire* **18**: 3–11.

Bosq M, Bertran P, Degeai JP, *et al*. 2020. Geochemical signature of sources, recycling and weathering in the Last Glacial loess from the Rhône Valley (southeast France) and comparison with other European regions. *Aeolian Research* **42**: 100561.

Bøtter-Jensen L, Bulur E, Murray AS, *et al*. 2002. Enhancements in luminescence measurement techniques. *Radiation Protection Dosimetry* **101**: 119-124.

Boycott AE. 1934. The Habitats of Land Mollusca in Britain. *Journal of Ecology* **22**: 1–38.

Cameron RAD, Palles-Clark MA. 1971. *Arianta arbustorum* (L.) on chalk downs in southern England. *Proceedings of the Malacological Society of London* **39**: 311–318.

Clark PU, Dyke AS, Shakun JD, *et al*. 2009. The Last Glacial Maximum. *Science* **325**: 710–714.

Commont V. 1913. Les hommes contemporains du Renne dans la Vallée de la Somme. *Mémoires de la Société des Antiquaires de Picardie* **37**: 207–638.

Duprat-Oualid F, Rius D, Bégeot C, *et al*. 2017. Vegetation response to abrupt climate changes in Western Europe from 45 to 14.7k cal a BP: the Bergsee lacustrine record (Black Forest, Germany). *Journal of Quaternary Science* **32**: 1008–1021.

Evans JG. 1972. *Land snails in archaeology*. Seminar Press: London & New York.

Fagnart JP, Coudret P, Antoine P, *et al*. 2013. Le Paléolithique supérieur ancien dans le Nord de la France. *Mémoires de la Société Préhistorique Française* **56**: 197–214.

Fankhauser A, McDermott F, Fleitmann D. 2016. Episodic speleothem deposition tracks the terrestrial impact of millennial-scale last glacial climate variability in SW Ireland. *Quaternary Science Reviews* **152**: 104–117.

Fischer P, Jöris O, Fitzsimmons KE, *et al*. 2020. Millennial-scale terrestrial ecosystem responses to Upper Pleistocene climatic changes: 4D-reconstruction of the Schwalbenberg Loess-Palaeosol-Sequence (Middle Rhine Valley, Germany). *Catena* **196**: 104913.

Flückiger J, Knutti R, White JWC, *et al*. 2008. Modeled seasonality of glacial abrupt climate events. *Climate Dynamics* **31**: 633–645.

Guérin G, Antoine P, Schmidt E, *et al*. 2017. Chronology of the Upper Pleistocene loess sequence of Havrincourt (France) and associated Palaeolithic occupations: A Bayesian approach from pedostratigraphy, OSL, radiocarbon, TL and ESR/U-series data. *Quaternary Geochronology* **42**: 15–30.

Guérin G, Mercier N, Adamiec G. 2011. Dose-rate conversion factors: update. *Ancient TL* **29**: 5–8.

Haesaerts P. 2009. Climatic signature and radiocarbon chronology of Middle and Late Pleniglacial loess from Eurasia: comparison with the marine and Greenland records. *Radiocarbon* **51**: 301–318.

Haesaerts P, Damblon F, Gerasimenko N, *et al*. 2016. The Late Pleistocene loess-palaeosol sequence of Middle Belgium. *Quaternary International* **411**: 25–43.

Horsák M, Juřičková L, Picka J. 2013. Měkkýši České a Slovenské republiky. Nakladatelství Kabourek: Zlín.

Jary Z, Ciszek D. 2013. Late Pleistocene loess–palaeosol sequences in Poland and western Ukraine. *Quaternary International* **296**: 37–50.

Kerney MP. 1963. Late-glacial deposits on the chalk of South-East England. *Philosophical transactions of the Royal Society of London Series B, Biological sciences* **246**: 203–254.

Kerney MP. 1971. A Middle Weichselian deposit at Halling, Kent. *Proceedings of the Geologists' Association* **82**: 1–10.

Kerney MP, Cameron RAD, Jungbluth JH. 1983. *Die Landschnecken Nord- und Mitteleuropas*. Verlag Paul Parey: Hamburg & Berlin.

Kuntz G, Dupuis C. 1972. *Carte géologique de la France à 1/50 000 (n° 46), Amiens (XXIII-8)*. Bureau de Recherches Géologiques et Minières: Orléans.

Lang A, Lindauer S, Kuhn R, *et al*. 1996. Procedures used for optically and infrared stimulated luminescence dating of sediments in Heidelberg. *Ancient TL* **14**: 7–11.

Lehmkuhl F, Nett JJ, Pötter S, *et al*. 2021. Loess landscapes of Europe – Mapping, geomorphology, and zonal differentiation. *Earth-Science Reviews* **215**: 103496.

Limondin-Lozouet N, Gauthier A. 2003. Biocénoses pléistocènes des séquences loessiques de Villiers-Adam (Val d'Oise, France) : études malacologiques et palynologiques. *Quaternaire* **14**: 237–252.

Ložek V. 1964. *Quartärmollusken der Tschechoslowakei*. Verlag der Tschechoslowakischen Akademie der Wissenschaften: Praha.

Ložek V. 1990. Molluscs in loess, their paleoecological significance and role in geochronology - Principles and methods. *Quaternary International* **7/8**: 71–79.

Luetscher M, Boch R, Sodemann H, *et al*. 2015. North Atlantic storm track changes during the Last Glacial Maximum recorded by Alpine speleothems. *Nature Communications* **6**: 1–6.

Meszner S, Kreutzer S, Fuchs M, *et al*. 2013. Late Pleistocene landscape dynamics in Saxony, Germany: Paleoenvironmental reconstruction using loess-paleosol sequences. *Quaternary International* **296**: 97–104.

Moine O. 2008. West-European malacofauna from loess deposits of the Weichselian Upper Pleniglacial: compilation and preliminary analysis of the database. *Quaternaire* **19**: 11–29.

Moine O. 2014. Weichselian Upper Pleniglacial environmental variability in north-western Europe reconstructed from terrestrial mollusc faunas and its relationship with the presence/absence of human settlements. *Quaternary International* **337**: 90–113.

Moine O, Antoine P, Deschodt L, *et al*. 2011. Enregistrements malacologiques à haute résolution dans les lœss et les gleys de toundra du Pléniglaciaire weichselien supérieur : premiers exemples du nord de la France. *Quaternaire* **22**: 307–325.

Moine O, Antoine P, Hatté C, *et al*. 2017. The impact of Last Glacial climate variability in west-European loess revealed by radiocarbon dating of fossil earthworm granules. *Proceedings of the National Academy of Sciences of the United States of America* **114**: 6209–6214.

Moine O, Rousseau D-D, Antoine P. 2008. The impact of Dansgaard-Oeschger cycles on the loessic environment and malacofauna of Nussloch (Germany) during the Upper Weichselian. *Quaternary Research* **70**: 91–104.

Murray AS, Wintle AG. 2000. Luminescence dating of quartz using an improved single aliquot regenerative-dose protocol. *Radiation Measurements* **32**: 57–73.

Murray AS, Wintle AG. 2003. The single aliquot regenerative dose protocol: potential for improvements in reliability. *Radiation Measurements* **37**: 377–381.

Nekola JC, Coles BF, Horsák M. 2015. Species assignment in Pupilla (Gastropoda: Pulmonata: Pupillidae): integration of DNA-sequence data and conchology. *Journal of Molluscan Studies* **81**: 196–216.

Paris C. 2020. *La période du Gravettien dans la zone loessique du Nord de la France. Traditions culturelles et dynamiques de peuplement*. Doctoral thesis, Université de Paris I Panthéon-Sorbonne: Paris.

Paris C, Antoine P, Auguste P, *et al*. 2019. Les gisements gravettiens d'Amiens-Renancourt 1 et 2 (Somme, France) : premières données palethnologiques. In *Préhistoire de l'Europe du Nord-Ouest : mobilité, climats et identités culturelles XXVIIIe Congrès préhistorique de France, Amiens 30 mai - 4 juin 2016 Volume 2 : Paléolithique supérieur ancien, Paléolithique final – Mésolithique*, Montoya C, Fagnart JP, Locht JL (eds). Société Préhistorique Française: Paris; 97–115.

Paris C, Deneuve E, Fagnart JP, *et al*. 2017. Premières observations sur le gisement gravettien à statuettes féminines d'Amiens-Renancourt 1 (Somme). *Bulletin de la Société Préhistorique Française* **114**: 423–444.

Paris C, Fagnart JP, Coudret P. 2013. Du Gravettien final dans le Nord de la France ? Nouvelles données à Amiens-Renancourt. *Bulletin de la Société Préhistorique Française* **110**: 123–126.

Prescott JR, Hutton JT. 1994. Cosmic ray contribution to dose rates for luminescence and ESR dating: large depths and long-term time variations. *Radiation Measurements* **23**: 497–500.

Puisségur JJ. 1976. *Mollusques continentaux quaternaires de Bourgogne. Significations stratigraphiques et climatiques. Rapports avec d'autres faunes boréales de France*. Doin: Paris.

Rasmussen SO, Bigler M, Blockley SP et al. 2014. A stratigraphic framework for abrupt climatic changes during the Last Glacial period based on three synchronized Greenland ice-core records: refining and extending the INTIMATE event stratigraphy. *Quaternary Science Reviews* **106**: 14–28.

Reimer PJ, Bard E, Bayliss A, *et al*. 2013. IntCal13 and Marine13 Radiocarbon Age Calibration Curves 0–50,000 Years cal BP. *Radiocarbon* **55**: 1869–1887.

Remy H. 1969. Würmzeitliche Molluskenfaunen aus Lößserien des Rheingaues und der nördlichen Rheinhessens. *Notizblatt des Hessischen Landesamtes für Bodenforschung zu Wiesbaden* **97**: 98–116.

Rousseau DD, Antoine P, Hatté C, *et al*. 2002. Abrupt millennial climatic changes from Nussloch (Germany) Upper Weichselian eolian records during the Last Glaciation. *Quaternary Science Reviews* **21**: 1577–1582.

Ruff M, Wacker L, Gäggeler HW, *et al*. 2007. A gas ion source for radiocarbon measurement at 200kV. *Radiocarbon* **49**: 307–314.

Schiermeyer J. 2000. *Würmzeitliche Lößmollusken aus der Eifel*. Doctoral thesis, Universität Düsseldorf: Düsseldorf.

Sirocko F, Knapp H, Dreher F, *et al*. 2016. The ELSA-Vegetation-Stack: Reconstruction of Landscape Evolution Zones (LEZ) from laminated Eifel maar sediments of the last 60,000 years. *Global and Planetary Change* **142**: 108–135.

Sprafke T, Schulte P, Meyer-Heintze S, *et al*. 2020. Paleoenvironments from robust loess stratigraphy using high-resolution color and grain-size data of the last glacial Krems-Wachtberg record (NE Austria). *Quaternary Science Reviews* **248**: 106602.

Stuiver M, Reimer PJ. 1993. Extended ^{14}C Data Base and Revised CALIB 3.0 ^{14}C Age Calibration Program. *Radiocarbon* **35**: 215–230.

Sümegi P, Molnár D, Gulyás S, *et al*. 2019. High-resolution proxy record of the environmental response to climatic variations during transition MIS3/MIS2 and MIS2 in Central Europe: The loess-paleosol sequence of Katymár brickyard (Hungary). *Quaternary International* **504**: 40–55.

Synal HA, Stocker M, Suter M. 2007. MICADAS: A new compact radiocarbon AMS system. *Nuclear Instruments and Methods in Physics Research. Section B, Beam Interactions with Materials and Atoms* **259**: 7–13.

Tisnérat-Laborde N, Thil F, Synal HA, *et al*. 2015. ECHoMICADAS: A new compact AMS system to measuring ^{14}C for Environment, Climate and Human Sciences. 22nd International Radiocarbon Conference 2015, Dakar, Sénégal: Books of abstracts. Université Cheikh Anta Diop, Dakar, PHYS-O.05.

Újvári G, Stevens T, Molnár M, *et al*. 2017. Coupled European and Greenland last glacial dust activity driven by North Atlantic climate. *Proceedings of the National Academy of Sciences of the United States of America* **114**: 10632–10638.

Walker DA, Walker MD. 1991. History and pattern of disturbance in Alaskan arctic terrestrial ecosystems: a hierarchical approach to analysing landscape change. *Journal of Applied Ecology* **28**: 244–276.

Welter-Schultes FW. 2012. European non-marine molluscs: a guide for species identification. Göttingen: Planet Poster.

Wessel P, Luis JF, Uieda L, *et al*. 2019. The Generic Mapping Tools version 6. *Geochemistry, Geophysics, Geosystems* **20**: 5556–5564.

Zech M, Kreutzer S, Zech R, *et al*. 2017. Comparative 14C and OSL dating of loess-paleosol sequences to evaluate post-depositional contamination of n-alkane biomarkers. *Quaternary Research* **87**: 180–189.

Zens J, Schulte P, Klasen N, *et al*. 2018. OSL chronologies of paleoenvironmental dynamics recorded by loess-paleosol sequences from Europe: Case studies from the Rhine-Meuse area and the Neckar Basin. *Palaeogeography, Palaeoclimatology, Palaeoecology* **509**: 105–125.

Zens J, Zeeden C, Römer W, *et al*. 2017. The Eltville Tephra (Western Europe) age revised: Integrating stratigraphic and dating information from different Last Glacial loess localities. *Palaeogeography, Palaeoclimatology, Palaeoecology* **466**: 240–251.

Unit / Depth	Sample	U (ppm)	Th (ppm)	K (%)	W (%)	Dα (Gy/ka)	Dβ (Gy/ka)	Dγ (Gy/ka)	Dcos. (Gy/ka)	Dann. (Gy/a)	De (Gy)	Age (ka)
7 / 3.65 m	REN1 14-03	2.72 ± 0.10	8.08 ± 0.10	1.16 ± 0.01	34.4 ± 3.4	0.40 ± 0.03	1.15 ± 0.05	0.75 ± 0.03	0.13 ± 0.01	2.43 ± 0.11	66.95 ± 1.41	27.6 ± 1.4
8 / 4.17 m	REN1 13-01	2.86 ± 0.17	8.48 ± 0.17	1.15 ± 0.02	32.0 ± 3.2	0.43 ± 0.03	1.19 ± 0.06	0.78 ± 0.04	0.12 ± 0.01	2.52 ± 0.12	70.41 ± 1.84	27.9 ± 1.5
8 / 4.17 m	REN1 14-04	3.26 ± 0.18	8.68 ± 0.20	1.14 ± 0.02	31.5 ± 3.2	0.47 ± 0.04	1.24 ± 0.06	0.83 ± 0.04	0.12 ± 0.01	2.65 ± 0.13	71.98 ± 1.82	27.2 ± 1.5
9 / 4.40 m	REN1 14-01	3.00 ± 0.18	8.48 ± 0.17	1.15 ± 0.02	30.8 ± 3.1	0.45 ± 0.03	1.22 ± 0.06	0.80 ± 0.04	0.12 ± 0.01	2.59 ± 0.12	73.49 ± 1.63	28.4 ± 1.5
11 / 5.10 m	REN1 14-02	2.82 ± 0.18	8.68 ± 0.20	1.17 ± 0.02	30.6 ± 3.1	0.44 ± 0.03	1.21 ± 0.06	0.80 ± 0.04	0.11 ± 0.01	2.56 ± 0.12	79.25 ± 1.67	31.0 ± 1.6
13 / 6.30 m	REN1 15-01	2.61 ± 0.19	8.07 ± 0.08	1.18 ± 0.02	23.3 ± 2.3	0.43 ± 0.03	1.26 ± 0.05	0.80 ± 0.03	0.12 ± 0.01	2.61 ± 0.11	68.42 ± 1.86	26.2 ± 1.3
13 / 6.30 m	REN1 15-01*	2.61 ± 0.19	8.07 ± 0.08	1.18 ± 0.02	44.7 ± 4.5*	0.36 ± 0.03	1.07 ± 0.06	0.69 ± 0.04	0.12 ± 0.01	2.24 ± 0.13	68.42 ± 1.86	30.5 ± 2.0

Table 1. OSL datings performed in Amiens-Renancourt 1 excavation. U, Th and K: elemental concentrations measured by gamma spectroscopy. W: Saturated water content. Dx: annual dose rates of α, β, γ and cosmic radiations, and equivalent dose. *The age of sample REN1 15-01 was recalculated with a more realistic water content from another sample that was physically close and taken on another profile of the site.

Material	Laboratory code	Sample / Depth (m)	^{14}C age (BP)	Calibrated age (a cal BP) [95.4% probability]	Median calibrated age	Source
Earthworm granules	Poz-73520	H: -15:-10 / 3.60-3.65	22190 ± 160	26036-26929	26415	this study
Earthworm granules	Poz-73521	H: -30:-25 / 3.75-3.80	22700 ± 160	26575-27389	27032	this study
Earthworm granules	SacA51278	H: -70:-65 / 4.15-4.20	23540 ± 150	27439-27907	27681	this study
Earthworm granules	Poz-73524	B: -50:-45	24610 ± 200	28154-29097	28645	this study
Earthworm granules	SacA51286	B: -70:-65 / 4.90-4.95	25220 ± 180	28811-29712	29262	this study
Earthworm granules	SacA46563	B: -95:-90 / 5.15-5.20	31410 ± 400	34584-36138	35313	this study
Earthworm granules	SacA46564	B: -125:-120 / 5.45-5.50	32540 ± 470	35472-38050	36569	this study
Earthworm granules	ECHo-3742.1.1/GifA 20375.1	A: -4.20 / ~6.70-6.90	30350 ± 490	33562-35271	34366	this study
Earthworm granules	ECHo-3742.1.2/GifA 20375.2	A: -4.20 / ~6.70-6.90	27160 ± 350	30667-31646	31142	this study
Earthworm granules	ECHo-3742.1.3/GifA 20375.3	A: -4.20 / ~6.70-6.90	39200 ± 1400	40926-45484	43138	this study
Bone	Beta-306063	Archaeological layer / 4.15-4.20	21890 ± 90	25898-26344	26092	Paris *et al.* (2013)
Bone	Lyon-9943/SacA32189	Archaeological layer / 4.15-4.20	22600 ± 170	26465-27333	26913	Paris *et al.* (2017)
Burnt bone	Lyon-9942/SacA32188	Archaeological layer / 4.15-4.20	23580 ± 180	27421-27996	27708	Paris *et al.* (2017)
Charcoal	Lyon-11659/SacA39279	Archaeological layer / 4.15-4.20	23250 ± 210	27158-27798	27500	Paris *et al.* (2017)
Bone	Lyon-632	Isolated bones found in unit 5 in a test pit about 100 m SSE of the site	23040 ± 220	26864-27721	27342	Fagnart *et al.* (2013)
Bone	Lyon-633		22360 ± 240	26089-27208	26647	Fagnart *et al.* (2013)

Table 2. Radiocarbon datings performed in Amiens-Renancourt 1 excavation and on a bone found in Renancourt 2000 test pit. Ages were calibrated with the software Calib 7.0.4 (Stuiver & Reimer, 1993) and the IntCal13 calibration curve (Reimer et al., 2013).

Ecological groups	2	5		7			7'	8	9	U			10					Molluscan record	
Samples	*Arianta arbustorum*	*Pupilla muscorum*	*Vallonia costata*	*Trochulus hispidus*	*Clausilia rugosa parvula*	*Punctum pygmaeum*	Slugs	*Succinella oblonga*	*Pupilla alpicola*	*Pupilla* sp.	cf. Chondrinidae	Total of terrestrials	*Pisidium* sp.	*Bithynia tentaculata*	Total of aquatics	Ostracods (valves)	Rodents (teeth, bones)	Cycles	Phases
H: 15:10	0	12	0	1	0	0	0	1	0	0	0	14	0	0	0	0	0		
H: 10:5	0	5	0	1	0	0	0	2	0	0	0	8	0	0	0	1	0	C7	I
H: 5:0	0	12	0	2	0	0	4	10	9	0	0	37	0	0	0	2	0		
H: 0:-5	0	0	0	1	0	0	1	8	10	0	0	20	1	0	1	5	0		
H: -5:-10	0	1	0	0	0	0	2	200	1	0	0	204	1	0	1	2	0		II
H: -10:-15	0	0	0	0	0	0	3	438	0	5	0	446	1	0	1	2	0	C6	
H: -15:-20	0	5	0	1	0	0	1	77	5	0	0	89	1	0	1	1	0		I
H: -20:-25	0	5	0	1	0	0	5	29	0	0	0	40	1	0	1	1	0		
H: -25:-30	0	0	0	1	0	0	5	91	12	0	0	109	2	0	2	4	0		II
H: -30:-35	1	24	0	1	1	0	5	97	0	0	0	129	0	0	0	1	0	C5	
H: -35:-40	0	12	1	2	0	0	17	45	12	0	0	89	1	0	1	0	0		I
H: -40:-45	0	24	0	1	0	0	9	98	0	0	0	132	1	0	1	4	0		
H: -45:-50	0	16	0	0	0	0	18	488	24	0	0	546	1	0	1	3	0		
H: -50:-55	0	7	0	0	0	0	33	499	57	0	0	596	0	0	0	1	0		IV
H: -55:-60	0	19	1	1	0	0	64	290	57	0	0	432	1	0	1	2	0		
H: -60:-65	0	92	0	0	0	0	51	174	372	0	0	689	0	0	0	1	0		III
H: -65:-69	0	7	0	1	0	0	14	102	40	0	0	164	0	0	0	1	0		
H: -70:-75	0	162	0	1	0	0	131	1245	542	0	0	2081	0	1	1	4	1		IIa
B: 0:-5	0	84	0	0	0	0	53	1309	249	0	0	1695	0	0	0	2	0	C4	
B: -5:-10	0	34	0	0	0	0	21	235	39	0	0	329	0	0	0	1	0		IIs
B: -10:-15	0	25	1	1	0	0	22	82	15	0	1	147	0	0	0	4	0		
B: -15:-20	0	13	0	1	0	0	22	26	25	0	0	87	0	0	0	7	0		
B: -20:-25	0	21	0	1	0	0	18	26	23	0	0	89	1	0	1	8	0		I
B: -25:-30	0	27	1	1	0	0	18	31	21	0	0	99	0	0	0	8	0		
B: -30:-35	0	38	0	1	0	0	31	35	47	0	0	152	2	0	2	13	0		
B: -35:-40	0	58	0	1	0	0	64	79	58	0	0	260	1	0	1	7	0		
B: -40:-45	0	162	0	7	0	0	276	265	194	0	0	904	1	0	1	7	0		IV
B: -45:-50	0	1320	0	28	0	0	503	791	1155	0	0	3797	1	0	1	2	0		IIId
B: -50:-55	0	507	0	2	0	0	293	1590	1463	0	0	3855	0	0	0	4	1		IIIh
B: -55:-60	0	310	0	3	0	1	146	2055	699	0	0	3214	2	0	2	1	0		
B: -60:-65	0	41	0	0	1	0	26	711	75	0	0	854	0	0	0	0	0	C3	IIa
B: -65:-70	0	6	0	0	0	0	6	58	5	0	0	75	0	0	0	5	0		
B: -70:-75	0	2	0	0	0	0	1	25	3	0	0	31	0	0	0	5	0		IIs
B: -75:-80	0	6	0	0	0	0	2	17	2	0	0	27	0	0	0	0	0		
B: -80:-85	0	6	0	0	0	0	0	13	4	0	0	23	0	0	0	0	0		I
B: -85:-90	0	7	0	0	0	0	0	6	5	0	0	18	0	0	0	4	0		
B: -90:-95	0	11	0	0	0	0	7	30	18	0	0	66	0	0	0	0	0		
B: -95:-100	0	4	0	0	0	0	2	20	16	0	0	42	0	0	0	2	0		II
B: -100:-105	0	4	0	3	0	0	0	6	5	0	0	18	0	0	0	1	0		
B: -105:-110	0	17	0	1	0	0	7	1	3	0	0	29	0	0	0	2	0	C2	
B: -110:-115	0	20	1	1	0	0	6	1	18	0	0	47	0	0	0	1	0		I
B: -115:-120	0	29	0	1	0	0	10	3	33	0	0	76	0	0	0	1	1		
B: -120:-125	0	66	1	2	0	0	42	9	87	0	0	207	1	0	1	0	0		IV
B: -125:-130	0	71	0	2	0	0	93	20	432	0	0	618	0	0	0	1	0	C1	III

Table 3. Molluscan taxa abundances of the Amiens-Renancourt 1 excavation. Ecological groups: half-forested (2), open (5), mesophilous (7), slugs (7'), hygrophilous (8), palustral (9), aquatics (10) and undetermined (U). See table 5 for the description of molluscan phase types.

ECOLOGICAL GROUP	TAXA	HABITAT	ECOLOGICAL REMARKS	REMARK'S AUTHOR
Hygrophilous (8)	*Succinella oblonga* (Draparnaud, 1801)	Wet stations with a sparse vegetation (humid meadows, swamps and near brooks).	It lives on "damp mud or rock surfaces, whether on the banks of rivers or lakes, or high up on screes".	Kerney (1971)
Palustral (9)	*Pupilla alpicola* (Charpentier, 1837)	Very wet mountain stations (fens with sparse vegetation, peat bogs, wet grasslands), preferentially in calcareous areas.		
Slugs (7')	Limacidae Lamarck, 1801 Milacidae Ellis, 1926	Various habitats, prefrentially with clayey soils retaining moisture and offering shelters and hiding places		
Open habitat (5)	*Pupilla muscorum* (Linnæus, 1758)	Open, dry and sunny, calcareous stations (dry meadows, sand dunes).	It tolerates "earth bare of vegetation" and "a considerable range of diurnal temperature as well".	Evans (1972)
	Vallonia costata (O.F. Müller, 1774)	Varied open, dry and humid, stations with stones; rarely found in woods or swamps.	It "prefers more stable grassland".	Kerney (1971)
Mesophilous (7)	*Trochulus hispidus* (Linnaeus, 1758)	Various moderately dry to humid stations (flood plains, marshy places, damp meadows, shrublands, light forest).	It is qualified as "relatively thermophilous"(*) and considered as an "early coloniser of damp broken ground before the development of a binding cover of vegetation"(**)	(*) Kerney (1963); (**) Kerney (1971)
	Punctum pygmaeum (Draparnaud, 1801)	fairly wet habitats with a developed vegetation cover (e.g. wood litter). Also in open stations and poor habitats offering a sufficient moisture or hiding places.	It is "characteristic of short-turf grassland and of open habitats where there is much bare ground"(*) and "often appear in places at an early successional stage" (**).	(*) Evans (1972); (**) Horsák *et al.* (2013)
	Clausilia rugosa parvula A. Férussac, 1807	Little humid to very dry shaded open stations with rocks and short vegetation. Rare in woods. Calciphile.		
Half-forested (2)	*Arianta arbustorum* (Linnaeus, 1758)	Very wet and vegetated stations. Also in sufficiently moist open stations. Cold resistant.	"It is commoner in river valley bottoms, (…) occurs more often in thick vegetation (…) and it is also favoured by steep north-facing slopes".	Cameron et al. (1971)
Aquatic (10)	*Pisidium* C. Pfeiffer, 1821	Various habitats: (periodic) swamps, standing and flowing waters		
	Bythinia tentaculata (Linnaeus, 1758)	Slowly flowing waters, but also in periodic pools on muddy bottom and plants when water dries out.		

869

870 **Table 4.** Taxa ecological preferences synthesised after (Boycott, 1934), Ložek (1964), Kerney
871 et al. (1983), Welter-Schultes (2012) and Horsák et al. (2013) and additional remarks. Taxa
872 are listed by ecological groups, which are ordered by decreasing importance in the site.
873 Taxonomical remarks: (i) while internal shells of Limacidae and Milacidae can be
874 distinguished, they cannot be identified at the species rank; (ii) according to their finely ribbed
875 microsculpture, the two apices of *Clausilia rugosa* (Draparnaud, 1801) found at Amiens-
876 Renancourt 1 were attributed to the sub-species *C. rugosa parvula* A. Férussac, 1807; (iii)
877 valves and fragments of *Pisidium* were too few to allow for a reliable identification at the
878 species rank; (iv) the single opercula attributed to this taxa cannot belong to another *Bithynia*
879 species such as *Bithynia leachii* (Sheppard, 1823).

880

Phases (and sub-phases)		Abundance	Richness	*Succinella oborga* (hygrophilous)	*Pupilla alpicola* (palustral)	*Pupilla muscorum* (open habitat)	Slugs (stable clayey soil)	*Trochulus hispidus* (mesophilous)	Vegetation-demanding taxa (*V. costata*, *C. r. parvula*, *P. pygmaeum*, *A. arbustorum*)
I: Stadial		MIN	(MIN)						
II: Stadial-interstadial transition	Start	↗	↗	↗(↗)	↗	↗	↗	(↗)	(↗)
	Acceleration	↗↗↗	↗	↗↗↗ (→ MAX)	↗↗↗	↗↗↗	↗↗	(↗)	(↗)
III: Interstadial optimum	Humid	MAX	↘	↘	↗(↗) MAX	(↗)	(↗)		(↘)
	Dry	MAX		↘(↘)	↘	(↗) MAX	↗	↗	
IV: Interstadial-stadial transition		↘↘(↘)		↘(↘)	↘(↘)	↘(↘)	↘(↘) MAX	(↘)	

Table 5. Definition criteria of molluscan phases identified at Amiens-Renancourt 1. Symbols are bracketed when changes do not systematically occur.

Figure 1. Location of Amiens-Renancourt 1 site and of other sites mentioned in this study. Legends: ice caps (light blue), modern coast lines (dashed lines), palaeo-coastlines at -120 m (plain line) around 27 ka according to Clark et al. (2009), elevation (level curves every 200 m from -120 m). Map realised with GMT 6 (Wessel et al., 2019) using a Mercator projection.

Figure 2. Local topographical context of the Amiens-Renancourt 1 site. Altimetry in metres NGF. The asterisk indicates the position of the Renancourt 2000 test pit. Map realised with version 3.4 of QGIS software (http://www.qgis.org) using the IGN BD Alti® at 5 m.

Figure 3. Pedostratigraphical record of Amiens-Renancourt 1 excavation with positions of all studied samples. The typology of pedological horizons follows the IUSS Working Group WRB (2015). H: upper profile; B: lower profile. Samples marked with a cross were not analysed due to the strongly reworked facies of the units concerned.

Figure 4. Granulometry, chronology and chronostratigraphy of the Amiens-Renancourt 1 loess sequence and correlations with the Nussloch loess sequence. Ages are laterally spaced according to their respective depths, except those of the archaeological layer that are artificially scattered on both sides of ^{14}C age H: -70:-65 for a better readability. ^{14}C ages Lyon-632 and Lyon-633 come from another profile (see table 2 and part 4.2). Rejected ages are marked by a dashed contour; they include H3 not figured. GI: Greenland interstadials. ET: Eltville tephra; LS: Lohne soil. Correlations between the Nussloch pedostratigraphy and the NGRIP were established in Moine et al. (2017). Dashed lines highlight correlations that are not supported by ^{14}C ages.

Figure 5. Diagrams of molluscan taxa absolute and relative abundances, and curves of several molluscan population parameters. Asterisks highlight successive specific abundance maxima.

Figure 6. Correlations between molluscan fauna parameters and grain size index variations of Amiens-Renancourt 1 and Nussloch loess sequences. NGRIP data: Rasmussen et al. (2014).

Figure 7. Correlation attempt between Amiens-Renancourt 1 molluscan phases and stadial-interstadial cycles. NGRIP data: Rasmussen et al. (2014). 7H (Sieben Hengste) data: Luetscher et al. (2015). The dashed vertical line symbolizes the equilibrium between the Mediterranean (depleted values) and the North Atlantic (enriched values) advection. NGRIP and 7H signals have been averaged to fit with the resolution (~100 years per sample) of Amiens-Renancourt 1 proxies.

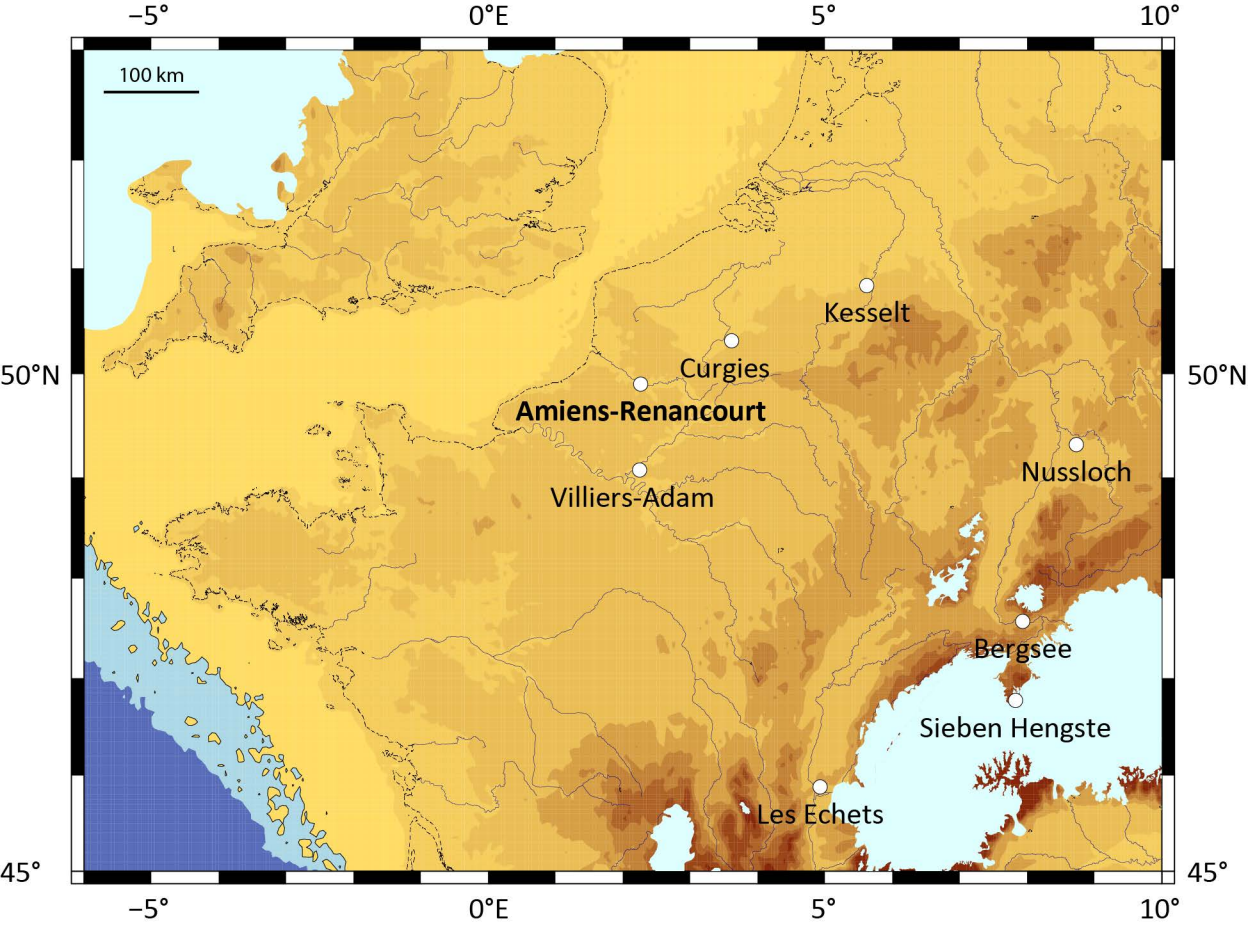
−5°
0°E
5°
10°
100 km
Kesselt
Curgies
Amiens-Renancourt
Villiers-Adam
Nussloch
Bergsee
Sieben Hengste
Les Echets
50°N
45°

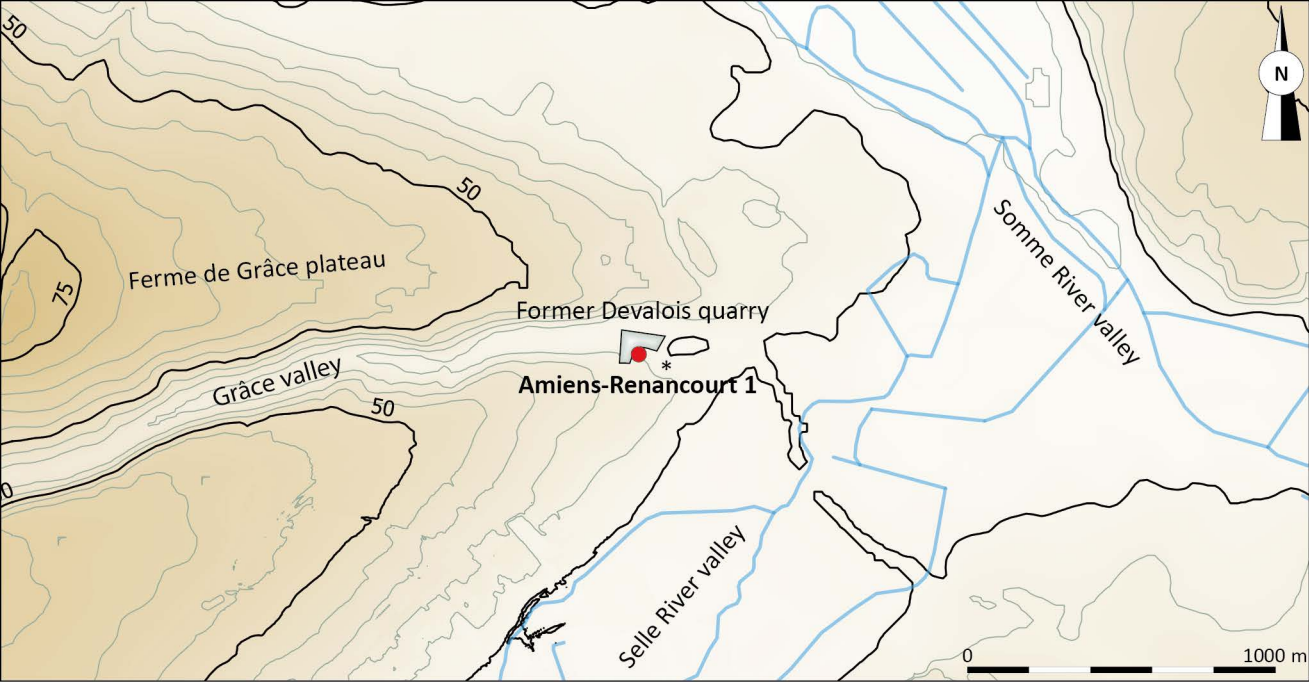
50
50
75
Ferme de Grâce plateau
Former Devalois quarry
Amiens-Renancourt 1
Grâce valley
50
Somme River valley
Selle River valley
N
0
1000 m

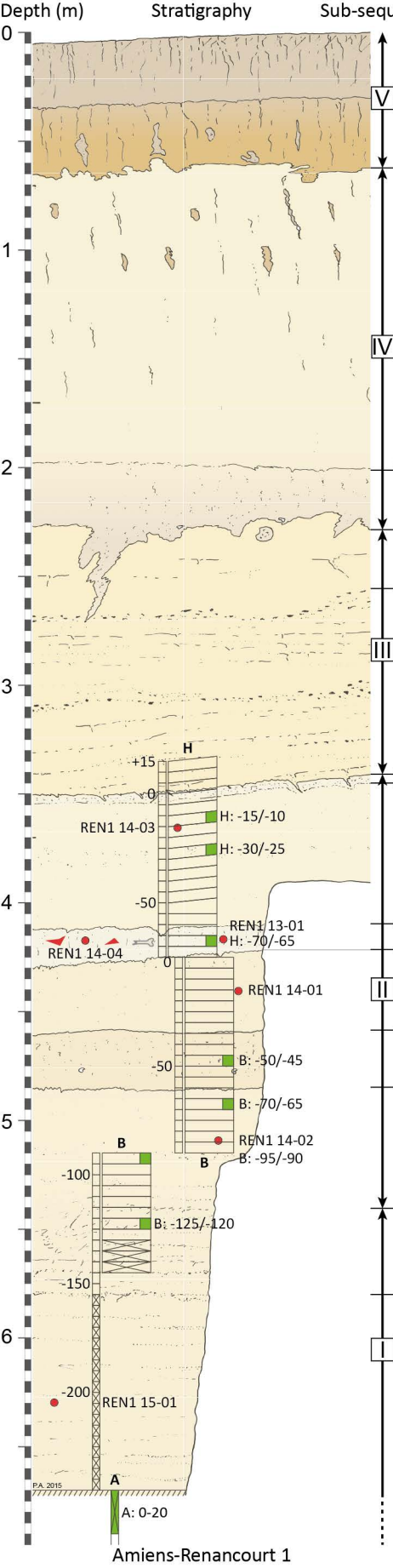

Unit # - Pedolithological description (**interpretation**)

0 - Brown-grey loam with granular structure, flints and scattered brick fragments; sharp lower boundary (**reworked AP horizon of topsoil**)

1 - Brown-red non calcareous clayey loam, compact, with large root tracks, numerous earthworm galleries and chambers infilled with material from the surface; irregular lower boundary (**truncated Bt horizon of topsoil**)

2 - Homogeneous light beige-greyish calcareous sandy loam with numerous large (Ø 1 mm) whitish secondary $CaCO_3$ on former root tracks (large rhyzoliths: Ø 1 cm) and pseudomycelium (Ø ≤ 1 mm), numerous subvertical earthworm galleries with clayey-humic coatings in the upper half of the unit; very diffuse and progressive lower boundary with unit 3 (**typical homogeneous calcareous loess**)

3 - Homogeneous grey-brownish slightly humic loam with numerous secondary $CaCO_3$ precipitation around root tracks (Ø 2-5 mm), pseudomycelium (Ø ≤ 1 mm) and scattered calcareous concretions (Ø 1-2 mm) at the base; fairly sharp but deformed lower boundary with locally the presence of a 0.5-m-deep ice-wedge cast strongly disturbed (**slightly humic tundra gley horizon with gelifluction tongues**)

4 - Light brown yellow calcareous sandy loess with rare sandy beds and micro-cracks deforming laminations, and scattered small ferro-manganese black patches; sharp lower boundary underlined by a gravel bed of small gelifracted flints (≤ 1 cm) and chalk granules (**calcareous loess with a few sand beds and cryodesiccation micro-cracks**)

5 - Compact brown-yellow calcareous laminated sandy loam with thin light grey beds (1-2 mm) and micro-cracks deforming laminations; a discontinuous layer of gelifracted flint and chalk granules separates this layer in two parts; clear lower boundary associated with microcracks (**laminated calcareous sandy loess with cryodesiccation micro-cracks**)

6 - Thin greyish loam with orange oxidised bands and stains and ferro-manganese concretions at the base; diffuse lower boundary (**thin tundra gley**)

7 - Homogeneous grey-beige calcareous loam with scattered pseudomycelium (**typical homogeneous calcareous loess**); presence of a thin diffuse horizon with oxidation stains in the median part (**micro-gley**)

8 - Light grey-yellow loam with greyish patches (hydromorphy) and subvertical orange oxidised lines underlined former root tracks and ferro-manganese concretions at the base; irregular lower boundary (**tundra gley**)

9 - Dense homogeneous beige-light grey calcareous loam with scattered ferro-manganese concretions (Ø < 1 mm) (**typical homogeneous calcareous loess**)

10 - Compact homogeneous brownish to brown-greyish calcareous loam with scattered small chalk granules and gelifracted flints; abundant pseudomycelium and numerous small ferro-manganese patches at the top; diffuse lower boundary (**slightly brownish horizon / weakly developed arctic brown soil**)

11 - Compact homogeneous light brown loam with rare scattered chalk granules and a few pseudomycelium; diffuse lower boundary (**typical homogeneous calcareous loess**); presence of a thin diffuse horizon with oxidation stains in the median part (**micro-gley**)

12 - Yellowish sandy loam with rather deformed greyish and orange beds and with numerous layers of chalk granules and scattered small gelifracted flints (~ 5 mm) reworked from the slope by hillwash processes (**geliflucted tundra gley complex incorporating chalk granules and gelifracted flints originating from the nearby slope**)

13 - Compact yellowish calcareous loam with sandy beds and rare chalk granules; base not reached (**loess reworked by hillwash processes**)
An auger survey (A) performed at the base of the profile revealed the presence of 1.7 m of sediment with a similar facies including increasing quantities of chalk granules and gelifracted flints in the lowermost 40 cm (only the upper metre is represented); the base of this unit lies 8.3-m-deep on a compact gravel of gelifracted flints on the top of which the borehole was stopped

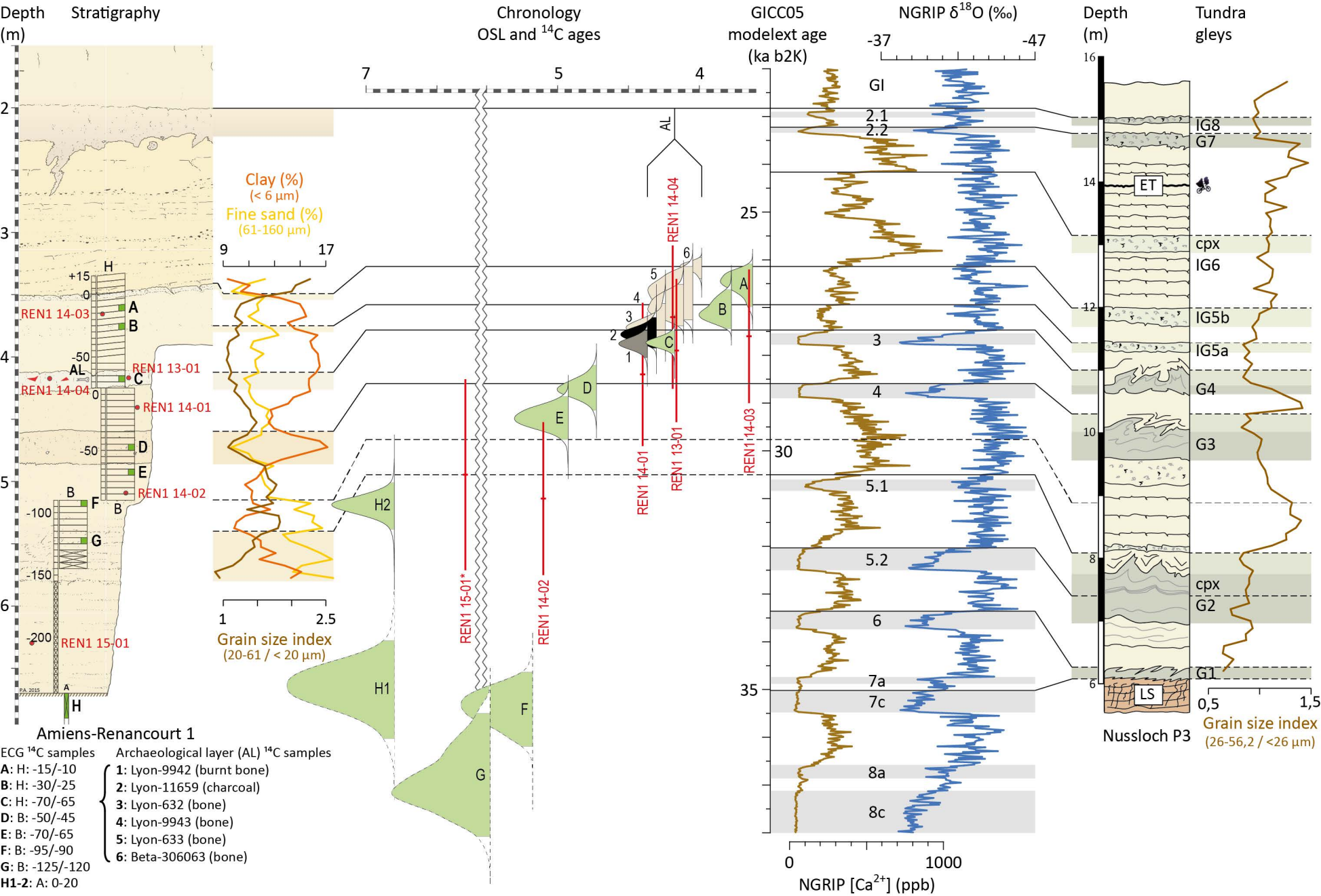
Depth (m)
Stratigraphy
Chronology OSL and ^{14}C ages
GICC05 modelext age (ka b2K)
NGRIP δ^{18}O (‰)
Depth (m)
Tundra gleys
Clay (%) (< 6 µm)
Fine sand (%) (61-160 µm)
Grain size index (20-61 / < 20 µm)
REN1 14-03
REN1 14-04
REN1 13-01
REN1 14-01
REN1 14-02
REN1 15-01
REN1 15-01*
AL
H
A
B
C
D
E
F
G
H1
H2
GI
2.1
2.2
3
4
5.1
5.2
6
7a
7c
8a
8c
NGRIP [Ca^{2+}] (ppb)
IG8
G7
ET
cpx
IG6
IG5b
IG5a
G4
G3
cpx
G2
G1
LS
Grain size index (26-56,2 / <26 µm)
Amiens-Renancourt 1
Nussloch P3
ECG ^{14}C samples
A: H: -15/-10
B: H: -30/-25
C: H: -70/-65
D: B: -50/-45
E: B: -70/-65
F: B: -95/-90
G: B: -125/-120
H1-2: A: 0-20
Archaeological layer (AL) ^{14}C samples
1: Lyon-9942 (burnt bone)
2: Lyon-11659 (charcoal)
3: Lyon-632 (bone)
4: Lyon-9943 (bone)
5: Lyon-633 (bone)
6: Beta-306063 (bone)

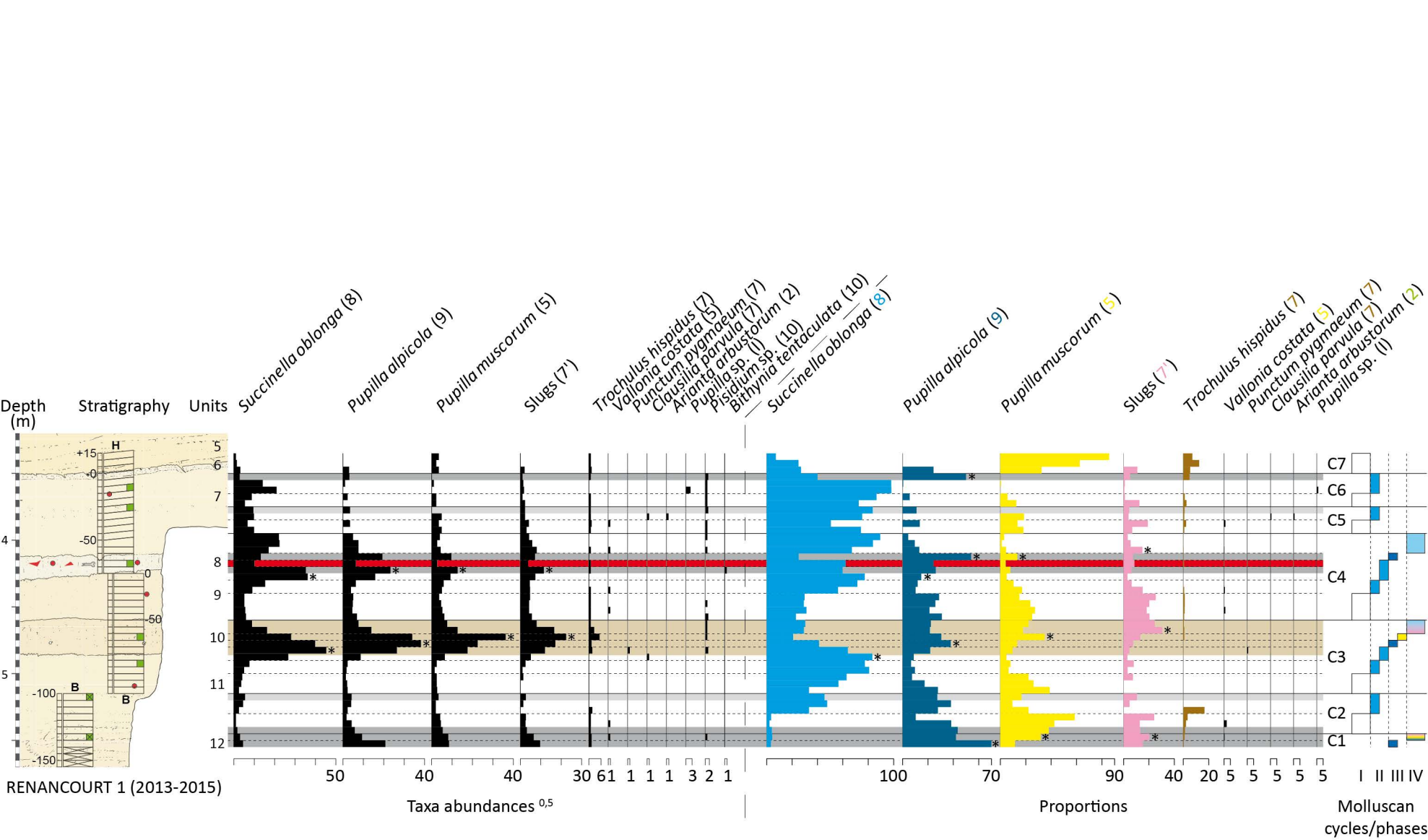
Depth (m)
Stratigraphy
Units
Succinella oblonga (8)
Pupilla alpicola (9)
Pupilla muscorum (5)
Slugs (7')
Trochulus hispidus (7)
Vallonia costata (5)
Punctum pygmaeum (7)
Clausilia parvula (7)
Arianta arbustorum (2)
Pupilla sp. (I)
Pisidium sp. (10)
Bithynia tentaculata (10)
Succinella oblonga (8)
Pupilla alpicola (9)
Pupilla muscorum (5)
Slugs (7')
Trochulus hispidus (7)
Vallonia costata (5)
Punctum pygmaeum (7)
Clausilia parvula (7)
Arianta arbustorum (2)
Pupilla sp. (I)
H
B
B
+15
0
-50
0
-50
-100
-150
4
5
5
6
7
8
9
10
11
12
C7
C6
C5
C4
C3
C2
C1
50
40
40
30
61
1
1
1
3
2
1
100
70
90
40
20
5
5
5
5
5
I
II
III
IV
Taxa abundances 0,5
Proportions
Molluscan cycles/phases
RENANCOURT 1 (2013-2015)

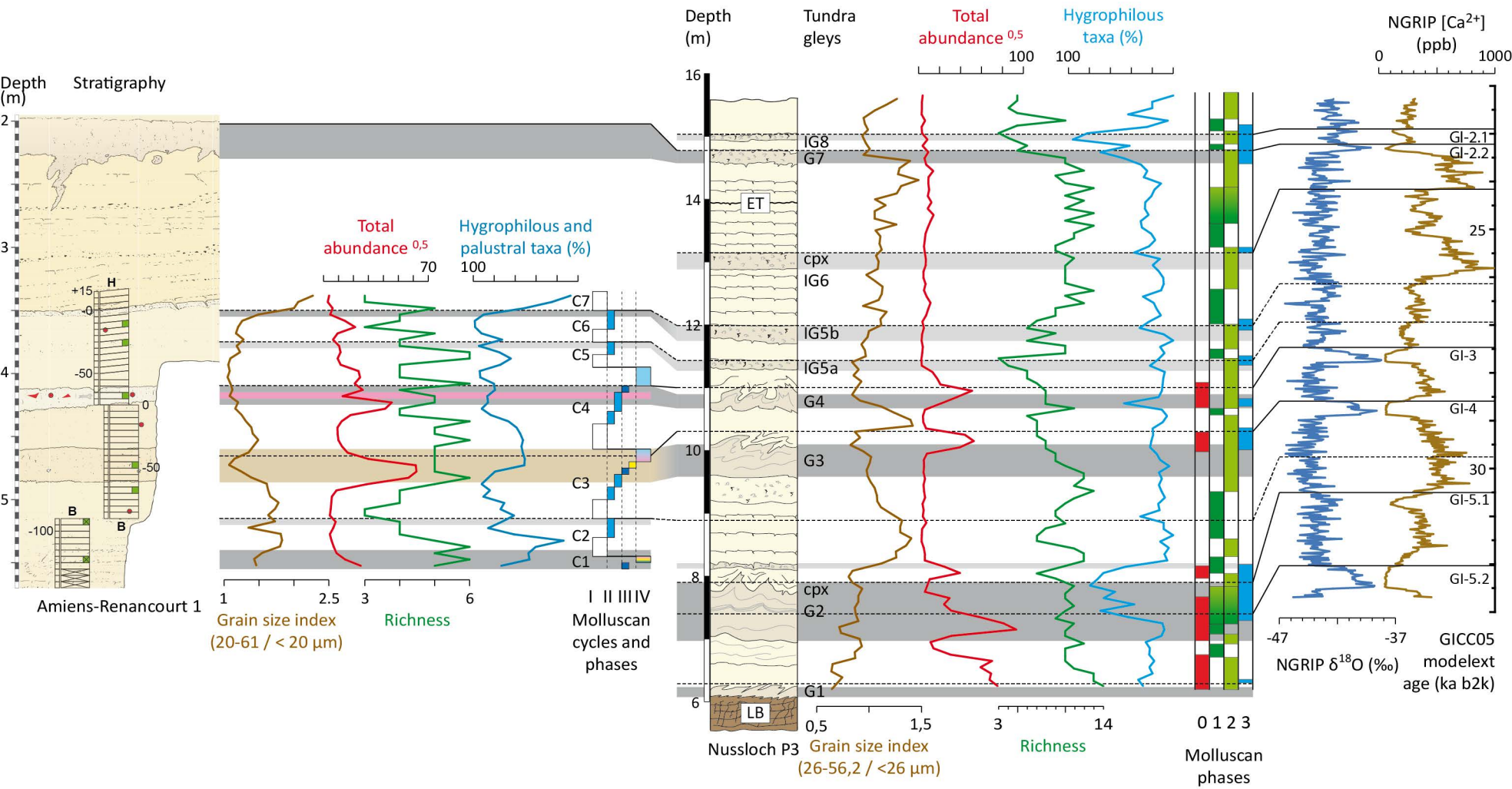
Depth (m)
Stratigraphy
Amiens-Renancourt 1
Total abundance 0,5
Hygrophilous and palustral taxa (%)
Grain size index (20-61 / < 20 µm)
Richness
C7
C6
C5
C4
C3
C2
C1
I II III IV
Molluscan cycles and phases
Depth (m)
Tundra gleys
Total abundance 0,5
Hygrophilous taxa (%)
IG8
G7
ET
cpx
IG6
IG5b
IG5a
G4
G3
cpx
G2
G1
LB
Nussloch P3
Grain size index (26-56,2 / <26 µm)
Richness
Molluscan phases
NGRIP [Ca2+] (ppb)
GI-2.1
GI-2.2
GI-3
GI-4
GI-5.1
GI-5.2
NGRIP δ18O (‰)
GICC05 modelext age (ka b2k)

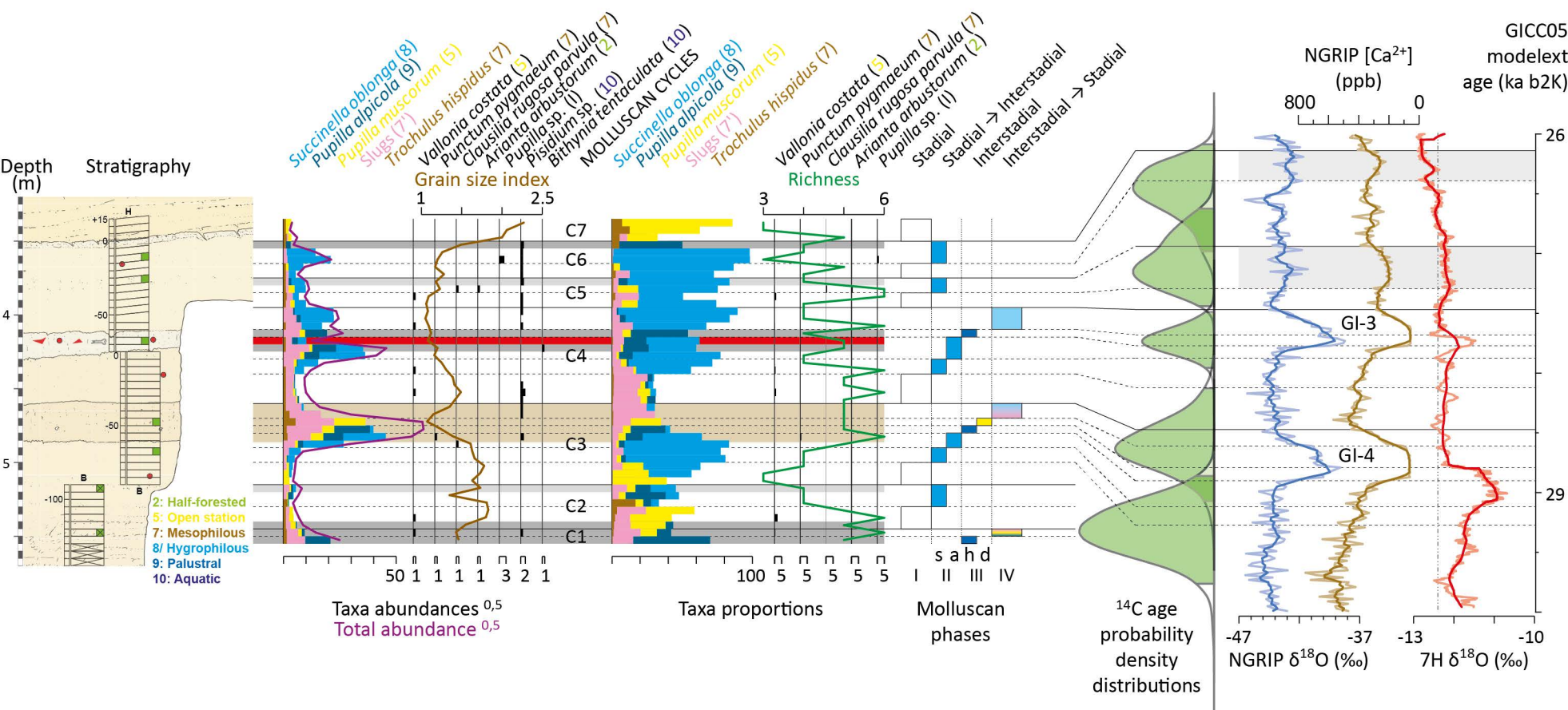
Depth (m)
Stratigraphy
2: Half-forested
5: Open station
7: Mesophilous
8/ Hygrophilous
9: Palustral
10: Aquatic
Succinella oblonga (8)
Pupilla alpicola (9)
Pupilla muscorum (5)
Slugs (7')
Trochulus hispidus (7)
Vallonia costata (5)
Punctum pygmaeum (7)
Clausilia rugosa parvula (7)
Ariantа arbustorum (2)
Pupilla sp. (I)
Pisidium sp. (10)
Bithynia tentaculata (10)
MOLLUSCAN CYCLES
Succinella oblonga (8)
Pupilla alpicola (9)
Pupilla muscorum (5)
Slugs (7')
Trochulus hispidus (7)
Vallonia costata (5)
Punctum pygmaeum (7)
Clausilia rugosa parvula (7)
Ariantа arbustorum (2)
Pupilla sp. (I)
Stadial
Stadial → Interstadial
Interstadial
Interstadial → Stadial
Grain size index
Richness
C7
C6
C5
C4
C3
C2
C1
Taxa abundances 0,5
Total abundance 0,5
Taxa proportions
Molluscan phases
s a h d
I II III IV
14C age probability density distributions
NGRIP [Ca2+] (ppb)
GICC05 modelext age (ka b2K)
GI-3
GI-4
NGRIP δ18O (‰)
7H δ18O (‰)